EUROPEAN ORGANISATION FOR NUCLEAR RESEARCH

ORGANISATION EUROPEENNE POUR LA RECHERCHE NUCLEAIRE

CERN - PS DIVISION

PS / LP / Note 95-09 (Tech)

A 10 GHz WALL CURRENT MONITOR

J.Durand (PS), T.Tardy (MT), M.Wurgel (PS)

Geneva, Switzerland
February 1995

The e^- beam is initialized by the fourth harmonic of a Nd:YLF laser giving pulses with a Full Width Half Maximum (FWHM) = 13 ps measured by autocorrelation or by a Nd:YAG laser with a typical FWHM = 6 ns within a 100 ms period. This latter laser is used to develop and qualify the photocathodes for the CTF.

The space-charge effect in the DC gun limits the e^- beam peak current to about 20 A at E_c = 100 keV.

A wideband high-sensitivity monitor is required to cover the dynamic range of the experiments.

The distance gun to WCM, e^- optic, and DC gun parameter values will result in e^- stretched bunches versus the laser pulse.

The WCM design has to be compatible with ultrahigh vacuum (UHV) conditions and withstand standard baking operation up to at least 150°C.

2.2 At the Clic Test Facility

The image current may be more than 1 kA with a 330 ps interval between the e^- bunches (FWHM = 8 ps measured with a streak camera).

As many as 48 bunches may coexist inside the same burst within a 100 ms period.

One useful measurement at CTF would be to compare the relative charge value of individual bunches.

A wideband ringing-free monitor with a low sensitivity is required.

In any case, the monitor has to be small enough to be inserted into a 40 mm diameter vacuum chamber. Requirements for UHV technology and baking are the same as previously described.

2.3 General remarks for the above applications

One needs to have in mind that, because e^- bunches are of picosecond duration, the response of the monitor will always be slower than the e^- beam, except for nanosecond applications at the Photoemission Laboratory.

Picosecond applications mean that the monitor will, unfortunately, be used on the slope of its transfer characteristic. This requires the widest ringing-free bandwidth at the monitor and an option to limit the bandwidth by an external absorbtive lowpass filter of known response (for instance a Gaussian LPF). Thus, the slope of the transfer characteristic of the monitor system would be more easily defined.

3 A WALL-CURRENT MONITOR SIMPLE MODEL

3.1 Influence of the electrical parameters

The WCM can be described simply (Fig. 2).

The capacitor C at the gap and the external loading resistor R_L will determine the high-frequency cut-off.

The length ℓ of the screening box is filled with a microwave absorber material. In addition, an inductance is obtained which determines the low-frequency cut-off.

EUROPEAN ORGANIZATION FOR NUCLEAR RESEARCH

A 10 GHz WALL-CURRENT MONITOR

J. Durand (PS), T. Tardy (MT), M.Wurgel (PS)

1 INTRODUCTION

Wall-current monitors (WCMs) are broadband devices often used for observation of the longitudinal profile of particle beams. In this note we would like to give information about the experience gained during the design and use of such a monitor at the PS/LP Photoemission Laboratory [1]. An attempted application for the Clic Test Facility (CTF) [2] will also be described.

As a particle beam travels along, it induces simultaneously on the wall of the vacuum chamber an image current which is the accurate representation of the charge distribution of the beam.

The wall-current monitor is basically a cut in the vacuum chamber to allow the measurement of the image current (Fig. 1).

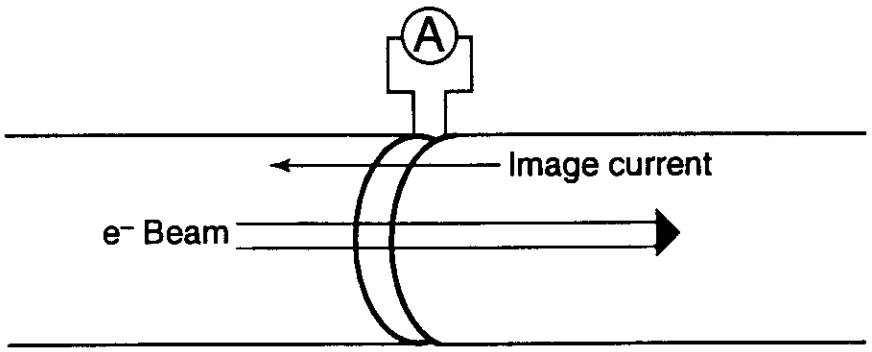

Fig. 1 A wall-current monitor is basically a cut in the vacuum chamber to allow the measurement of the image current

If a resistor is put across the gap thus formed, the monitor voltage output is proportional to the instantaneous image current if the response of the monitor is faster than the bunch length. Also the wall-current monitor is independent of the beam position if the connections at the gap are distributed all around its circumference.

The wall-current monitor described here takes into account a lot of ideas developed in Ref. [3].

2 ENVIRONMENT AND RELATED MONITOR CHARACTERISTICS

2.1 At the Photoemission Laboratory

This environment was previously described [4].

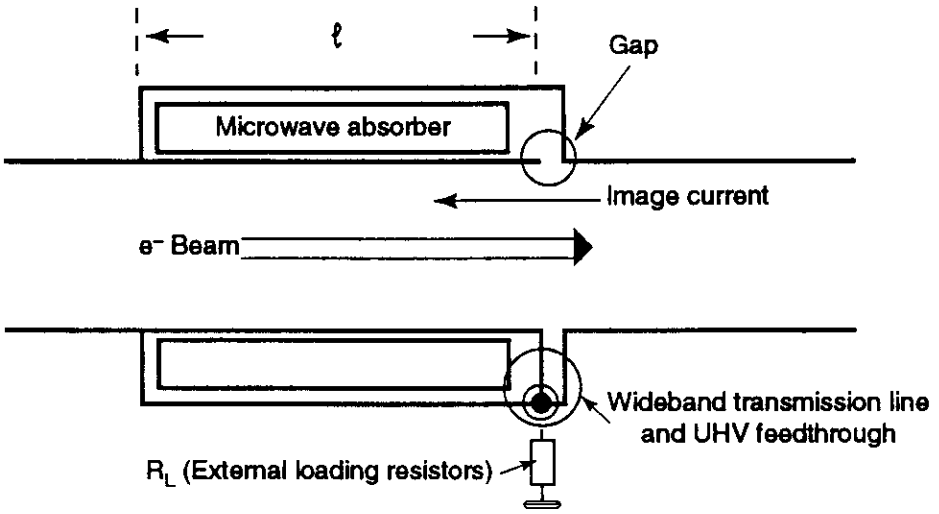

Fig. 2 The wall-current monitor

The beam is taken as an ideal current source (I_b) [3].

A simple model of the wall-current monitor can be made (Fig. 3) and simulated with a computer program [SPICE™] (Fig. 4).

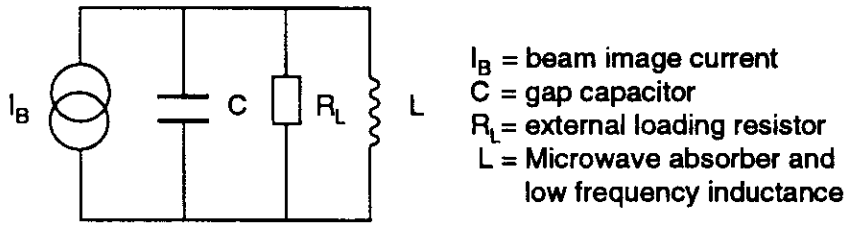

Fig. 3 A WCM simple model

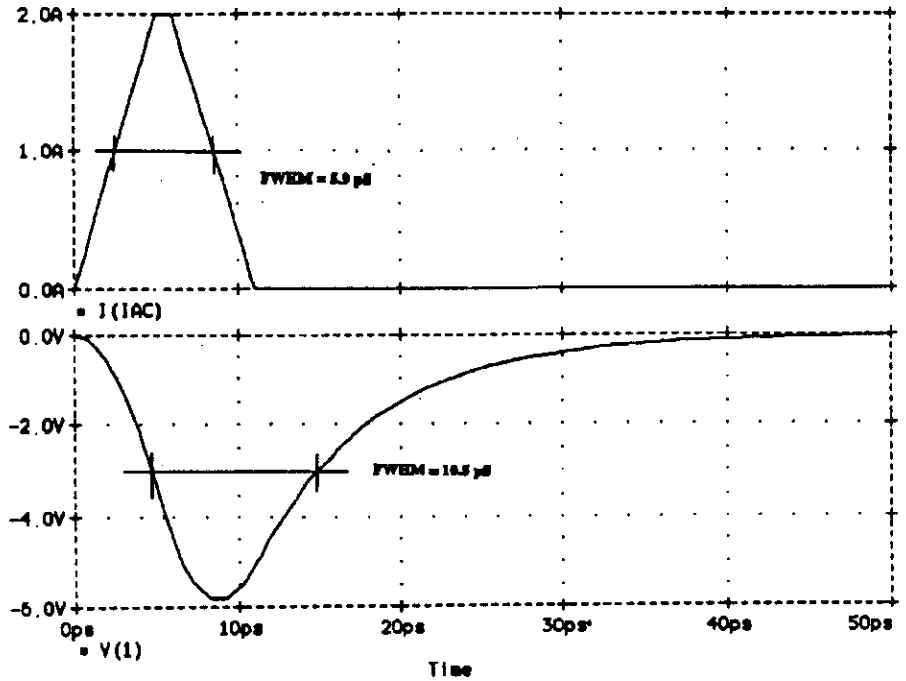

Fig. 4 The WCM simulation with SPICE™. Upper trace: Beam simulation (I_b). Lower trace: U (R_L) (WCM output). Parameter values for the simulation are the following. Vacuum chamber dimensions: external diameter = 44.5 mm, internal diameter = 40.5 mm; equivalent surface at the gap = 267×10^{-6} m^2; gap capacitor (neglecting fringing fields) = $\varepsilon_0\ \varepsilon_r$ S/d = 1.2 pF, with d = 2 mm and $\varepsilon_r = \varepsilon_0$ (vacuum conditions). Inductance L = 1 μH. R_L = 50/6 = 6.25 Ω. I_b = image current.
Note that the I_b symmetry is lost at the R_L output. The speed of the system remains high.

A question which immediately arises is to quantify the loss of the monitor performances by the transmission line between the gap and the external loading resistor R_L.

We suppose now the use of a subminiature vacuum feedthrough with an equivalent capacitative reactance of 0.42 pF.

A look at the monitor architecture shows an inductance of 2 nH for a 4 mm long connection (Appendix 1) needed between the gap and the feedthroughs.

Figure 5 shows the simulation result using eight 50 Ω outputs, each with a 2 nH inductance just before the capacitative feedthrough. The ringing (T = 100 ps, F = 10 GHz) makes such a monitor unsuitable for the application.

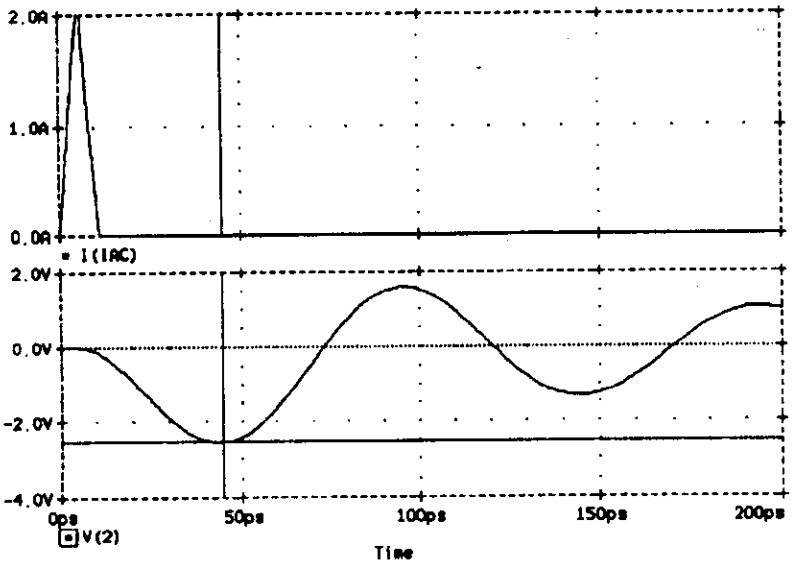

Fig. 5 Upper trace: I_b. Lower trace: WCM output. Ringing is the consequence of a short 4 mm connection between the gap and the eight outputs. T = 100 ps, F_{osc} = 10 GHz.

If a serial damping resistor is introduced with the connection, a nearly usable output is obtained to the detriment of the FWHM which now reaches a value of 33 ps (Fig. 6). From our experience such a solution is to be avoided.

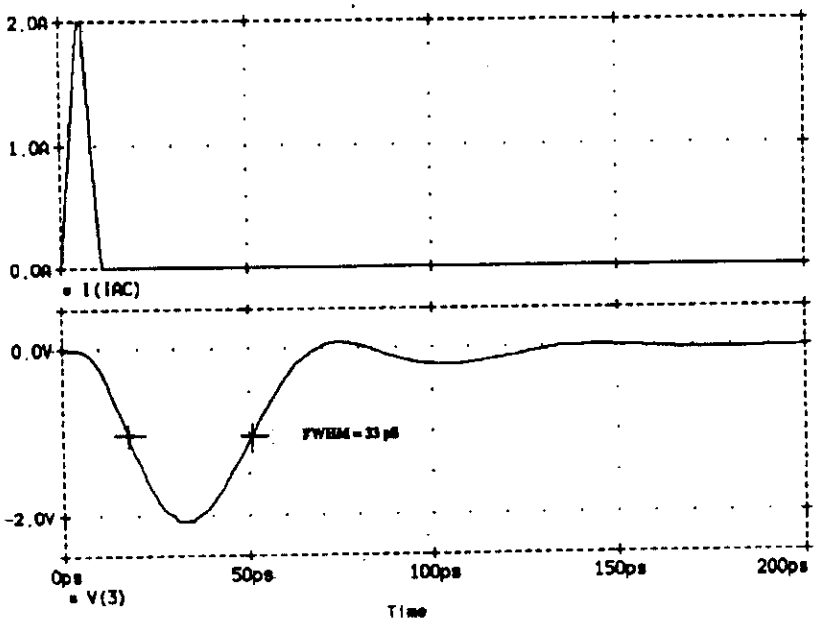

Fig. 6 Upper trace: I_b. Lower trace: WCM output. Damping the 10 GHz ringing with serial back-matching 50 Ω resistors.

3.2 Influence of the gap width

Because of the time involved with such an application, the gap dimension has to be taken into account [5].

3.2.1 At the Photoemission Laboratory

$\gamma = (E_0 + E_c)/E_c = 1.195$ with $E_0 = 511$ keV and $E_c = 100$ keV

$\beta = 0.547$

$1/v = 6.087$ ps/mm.

A 2 mm gap corresponds to a flight time of 12 ps.

3.2.2 At the Clic Test Facility

Because of the energy involved ($E_c > 10$ MeV) e^- particles are relativistic.

$$1/v = 1/c = 3.3 \text{ ps/mm} .$$

A 2 mm gap corresponds to a flight time of 6.6 ps.

It should be pointed out that the simulation done with SPICE™ does not take into account the β effect as well as standing waves on the transmission lines between the gap and the vacuum feedthrough.

4 DESIGN AND EVALUATION OF A HOME-MADE WCM PROTOTYPE

This wall-current monitor is built using standard-sized brass tubing (Fig. 7) to confirm practically the trend of the SPICE™ simulations.

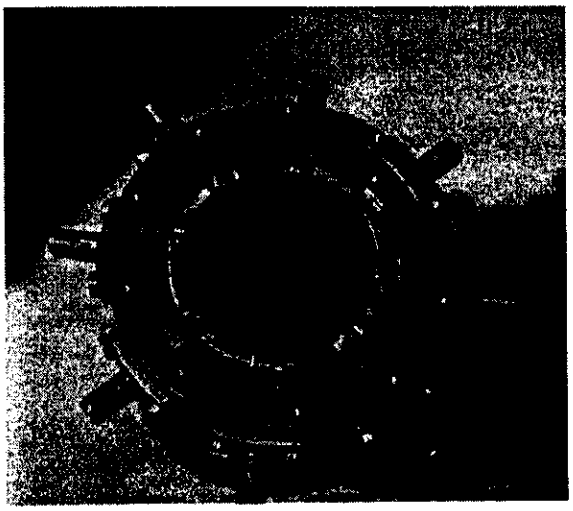

Fig. 7 The home-made wall-current monitor

The internal dimensions are chosen close to the true specification for a UHV compatible design. The monitor architecture is shown at Fig. 8.

The eight connections are distributed all around the gap using 50 Ω microstrip technology [3].

Tiles of the ZN type (Eccosorb NZ2 from Emerson and Cumming) are used as microwave absorber. They are machined to the suitable circular shape (external diameter 60 mm, internal diameter 40.5 mm) to fill as close as possible the shielded area sump volume. Some additional characteristics for these tiles are given in Fig. 9.

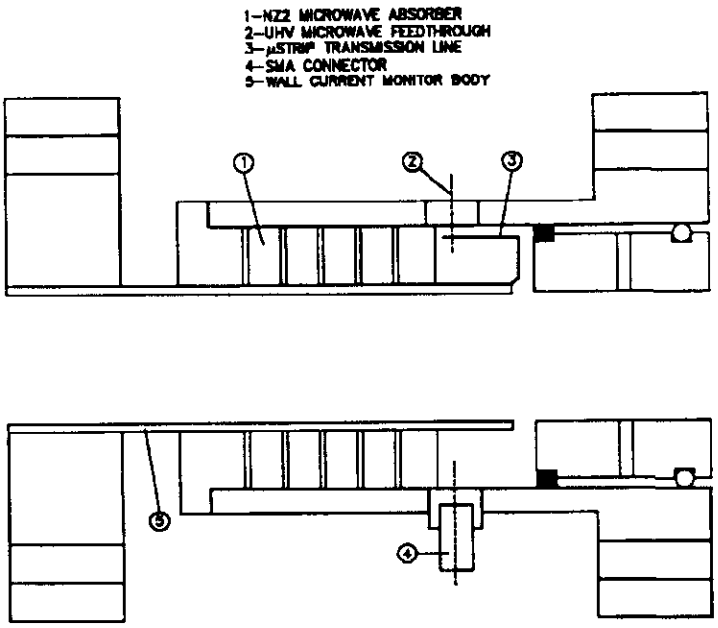

Fig. 8 The 10 GHz wall-current architecture

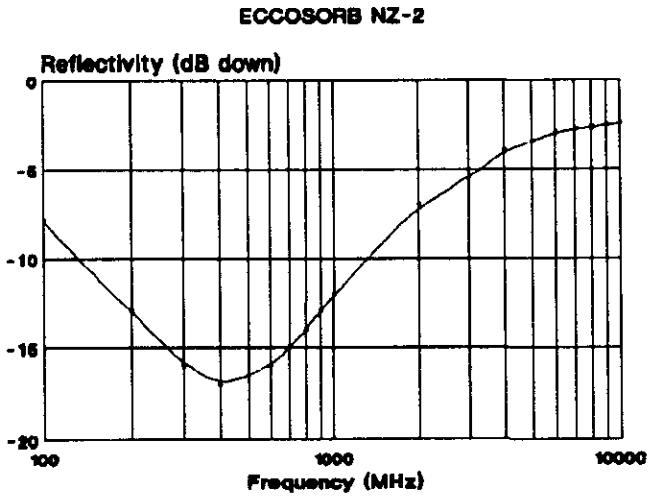

Frequency range (Mhz)	50–3000
Physical form	Flat tile
Nominal length and width (cm)	6.0 × 6.0
Nominal thickness (cm)	0.64
Nominal Wt. (kg/m^2)	32
Basic material	Sintered ferrite
Colour	Black
Service temperature (°C)	–54 to +260
Power handling (watts/cm^2)	3.1

Fig. 9 Attenuation of the NZ2 tiles using reflectivity measurement

The overall length of the sump housing five slides of NZ2 absorber is about 70 mm. So, the $\lambda/4$ resonance is in the GHz range, well inside the best absorbtion behaviour of this microwave absorber. The measured inductance at 10 kHz is:

256 nH without the NZ2 tiles in the sump,

816 nH with five NZ2 tiles in the sump.

The time constant $\tau = L/R = 130$ ns gives the possibility to operate the wall-current monitor with a laser FWHM $\leq$ 13 ns with a negligible drift of the base line as specified.

Combining the eight wall-current monitor outputs is done on a binary basis with a 50 Ω fixed load at each of the combining nodes [6]. Because delay errors on the combined paths may induce time dispersion, all the 50 Ω semirigid coaxial lines are cut accurately using standard S11 phase measurement by a HP8409C network analyser. The path attenuation is 0.4 dB at 10 GHz in the combiner.

The vacuum feedthrough used is a miniature device from CICE built for pacemaker applications (Fig. 10). This feedthrough is inserted into the body wall of the WCM to obtain a transmission line as close as possible to 50 Ω. An attempt at characterization is done by interfacing the CICE feedthrough with SMA 12.4 GHz connectors (Fig. 11).

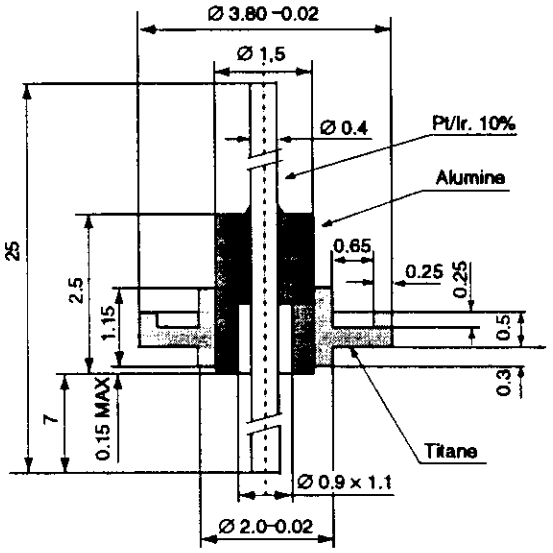

Fig. 10 The miniature CICE feedthrough. With the kind authorization of Marc Gaillard/CICE.

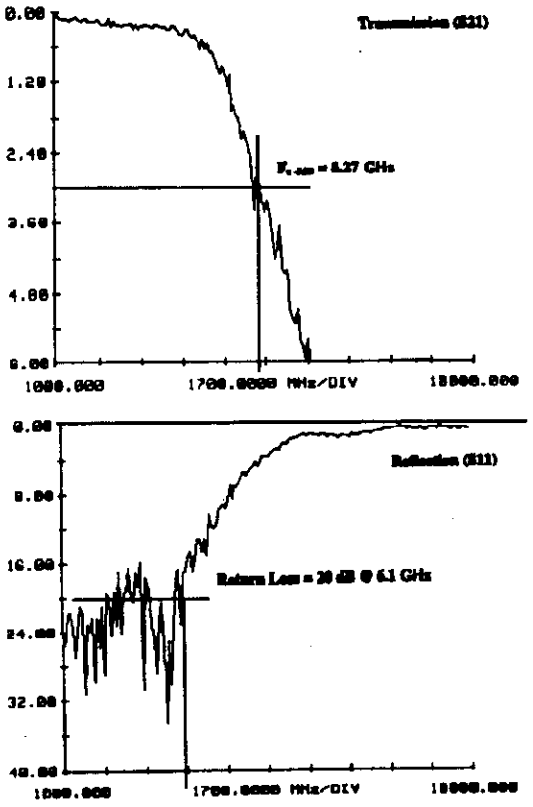

Fig. 11 S21 and S11 measurements of the CICE feedthrough inserted between two 12.4 GHz SMA connectors. Top: transmission characteristic (S21). Bottom: reflection characteristic (S11).

Figure 12 shows how the CICE feedthrough is inserted into the body wall of the home-made wall-current monitor. The outside circumference of the CICE feedthrough is glued using Araldite™ doped with silver as a substitute for soldering.

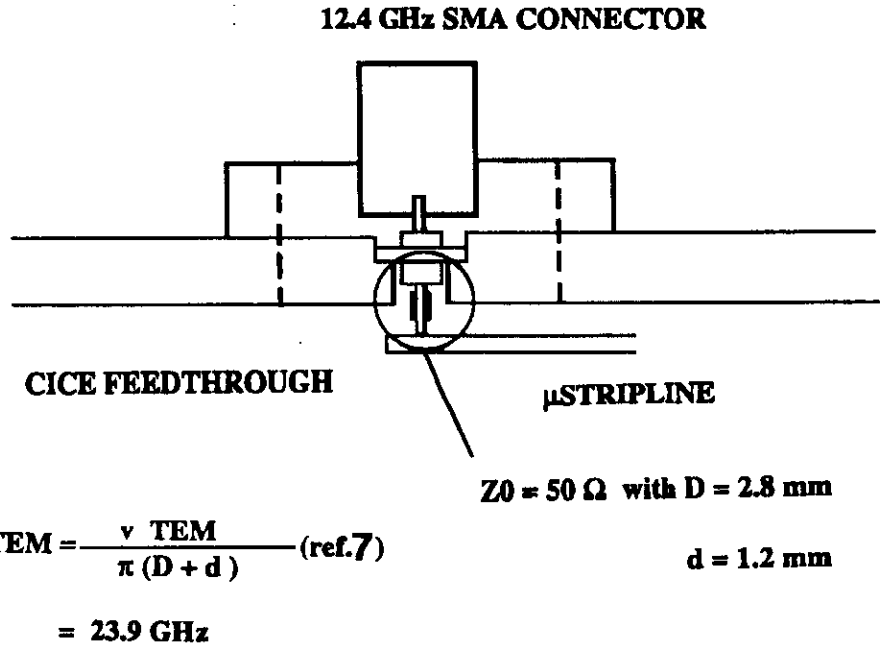

Fig. 12 Fitting the CICE feedthrough inside the wall of the home-made WCM

The size of the 50 Ω lines are defined using the Hammerstadt equations [8] solved by a QuickBASIC program [9] (Fig. 13).

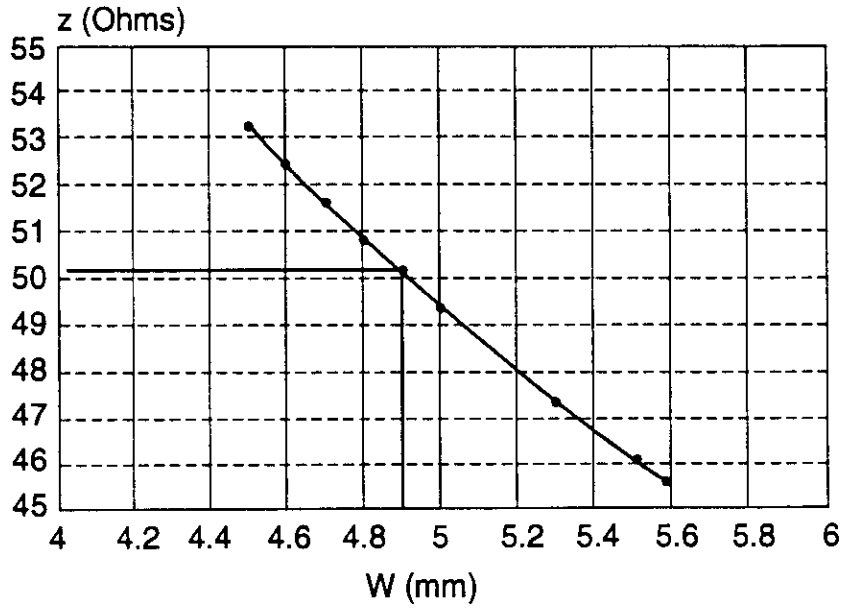

Fig. 13 Characteristic impedance of a microstrip line versus line width. Microstrip thickness = 1 mm. Microstrip-to-ground distance = 1 mm.

The whole wideband transmission system (SMA connector–CICE feedthrough–microstrip) is tested under Time Domain Reflectometry (TDR) conditions (HP54124T: 33 ps 10–90% rise time) (Fig. 14). Some particular locations have to be underlined, keeping in mind that this composite transmission system uses dielectric materials as varied as PTFE ($E_r = 2.1$), 98% Al_2O_3 ($E_r = 9.5$ at 10 GHz [10]), and vacuum ($E_r = 1$):

- SMA to CICE transition, VSWR = +6% (inductive), must be improved to limit the low-pass function by shortening the length of the connections;
- CICE feedthrough, VSWR = –4.5% (capacitative);
- CICE feedthrough to microstrip transition, VSWR = +16.5% (some further iterative improvements bring this location in the range of VSWR = +6%).

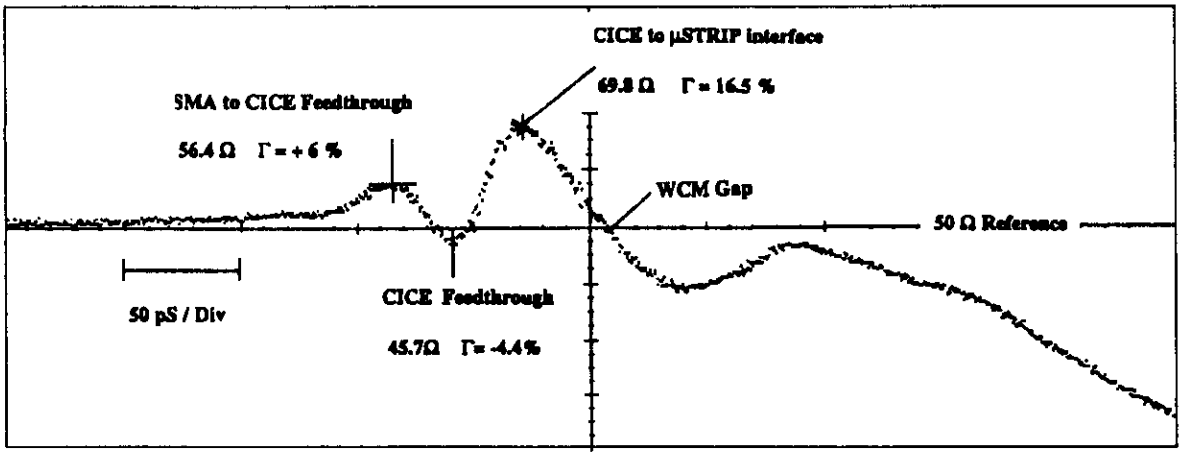

Fig. 14 Time domain reflectometry measurement from the SMA connector to the gap

No attempt at using the 10 ps Bracewell transform facility included inside the HP54124T was made, in spite of the small size of the CICE feedthrough [11].

Finally, this home-made wall-current monitor is inserted into a 40 mm diameter test bench (Fig. 15).

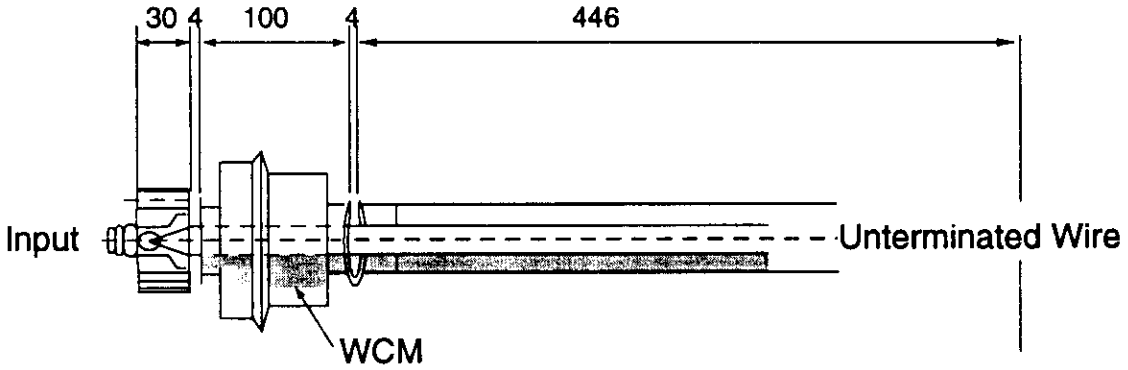

Fig. 15 This test bench uses a 0.5 mm diameter tight wire inside the 40 mm diameter vacuum chamber. This hardware time-gating technique does not use termination at the end of the wire. The beam simulation signal is the HP54124T TDR step generator. The observation is done with the 34 GHz input (T_r = 10.2 ps).

Figure 16 gives the rise time of the WCM extracted from the known response of the measurement system:

$$T_{r_{WCM}} = \sqrt{\left(T_{r_{tot}}\right)^2 - \left(T_{r_{meas}}\right)^2}\,.$$

The WCM is now inserted into a 50 Ω TEM test bench [12]. This test set is bandwidth-limited because of moding (first mode = TE11).

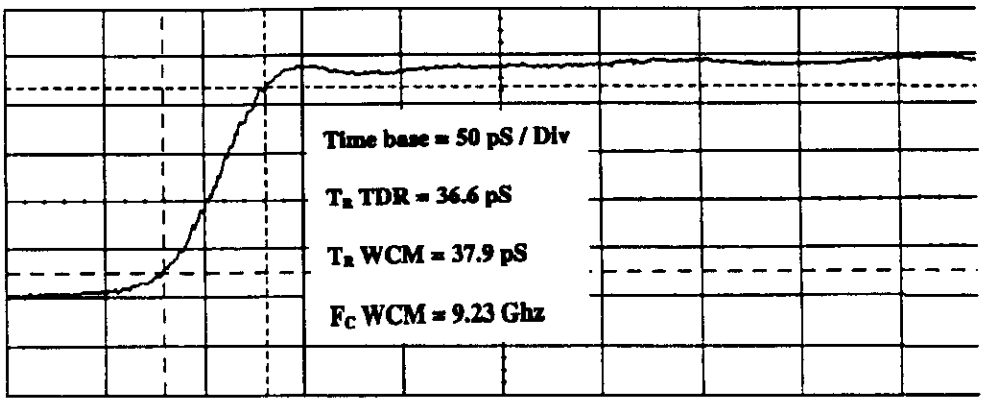

Fig. 16 The WCM response under TDR step conditions

The wavelength cut-off λ_c (combination of TEM00 and TE, TM modes) is:

$$\lambda_c = 2\pi R_m \left[1 - \frac{1}{6}\left(\frac{t}{2R_m}\right)^2 - \frac{7}{120}\left(\frac{t}{2R_m}\right)^4 \right] \quad \text{Ref. [13]}$$

with $R_m = (d + D)/2$
$t = D - d$
$D = 40.5$ mm
$d = 17.6$ mm

$$\lambda_c = 177 \text{ m} \Rightarrow F_c = 1.69 \text{ GHz (end of TEM00 only).}$$

Under these conditions, the transfer impedance of the WCM is measured to be:

$$|Z_{WCM}| = 4.3\ \Omega$$

and the time constant $\tau = 108$ ns (Fig. 17).

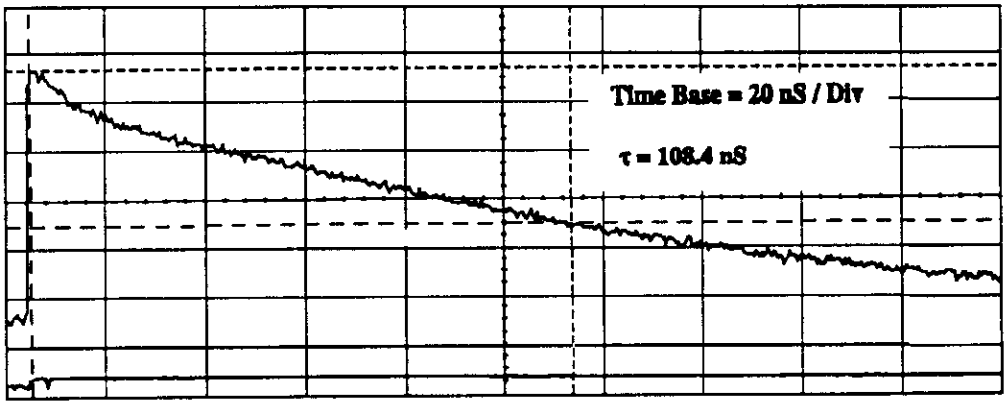

Fig. 17 τ = L/R measured on the 50 Ω TEM00 test bench

This approach confirms the simple model previously simulated with SPICE™ and the possibility of designing a wall-current monitor effective from 1 MHz up to 10 GHz.

5 THE CICE MINIATURE VACUUM FEEDTHROUGH

Seen by chance for the first time at the 1993 exhibition 'La France au CERN', this device seems to be a good candidate for microwave applications because of its small size (Fig. 10).

To do the analysis for a 50 Ω matching, one has to divide the feedthrough into three different parts (Fig. 18) [14]. The analysis is done using Ref. [15] for the upper and lower part of the feedthrough (transmission line with two coaxial dielectric constants). The middle part is assumed to be with the standard coaxial line equation:

$$Z_0 = (138/\sqrt{E_r}) \log_{10} (D/d) .$$

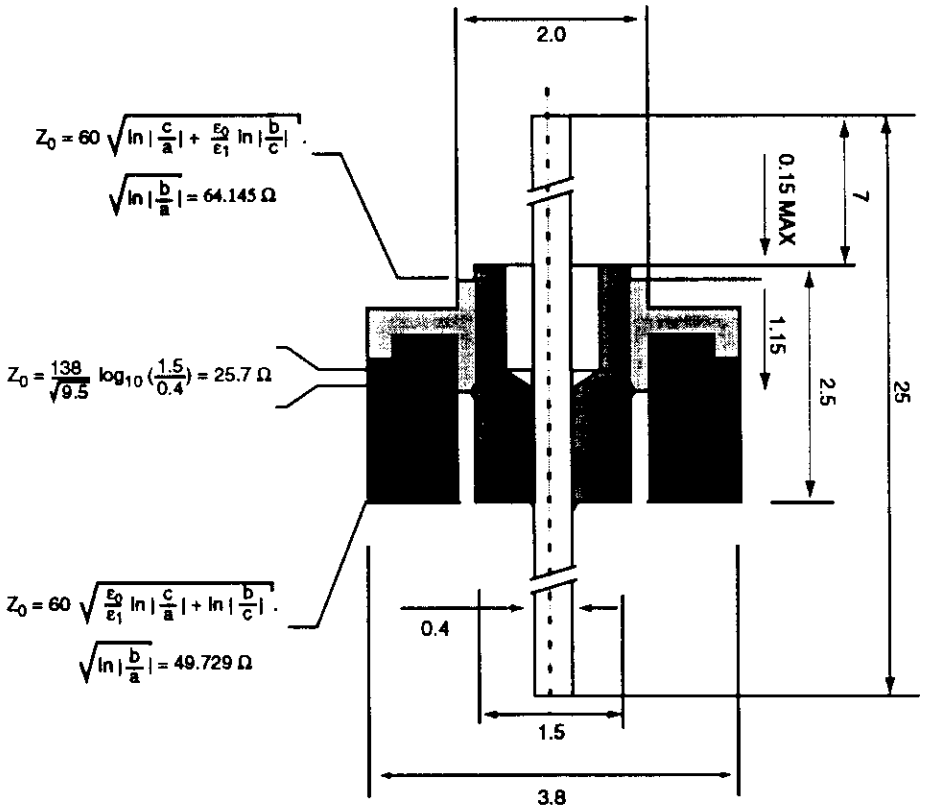

Fig. 18 Characteristic impedance of the CICE feedthrough

a) The upper part

The 0.4 mm diameter wire is folded to mate with a machined female-to-female SMA adaptor.

The length of the $Z_0 = 64\ \Omega$ section is about 1 mm. The SMA adaptor has to be as close as possible to the CICE feedthrough ground.

b) The middle part

The length of the $Z_0 = 25.7\ \Omega$ section is 0.25 mm with a relative velocity

$$v = 1/\sqrt{(E_r)} = 0.324\ c ,$$

which means a transit time of 2.5 ps at this location.

The equivalent capacitor is:

$$C = \frac{0.241\ E_r}{\log_{10}(D/d)}\ 10^{-12}\ \text{F/m} = 0.1\ \text{pF}\quad \text{Ref. [7].}$$

c) The lower part

The length of the $Z_0 = 49\ \Omega$ section is 1.4 mm and is obtained by inserting the feedthrough into a small ring of conducting material with an internal diameter of 2 mm (Figs. 19 and 20).

Fig. 19 The CICE feedthrough alone (right) and inserted inside the coaxial adaptor (left)

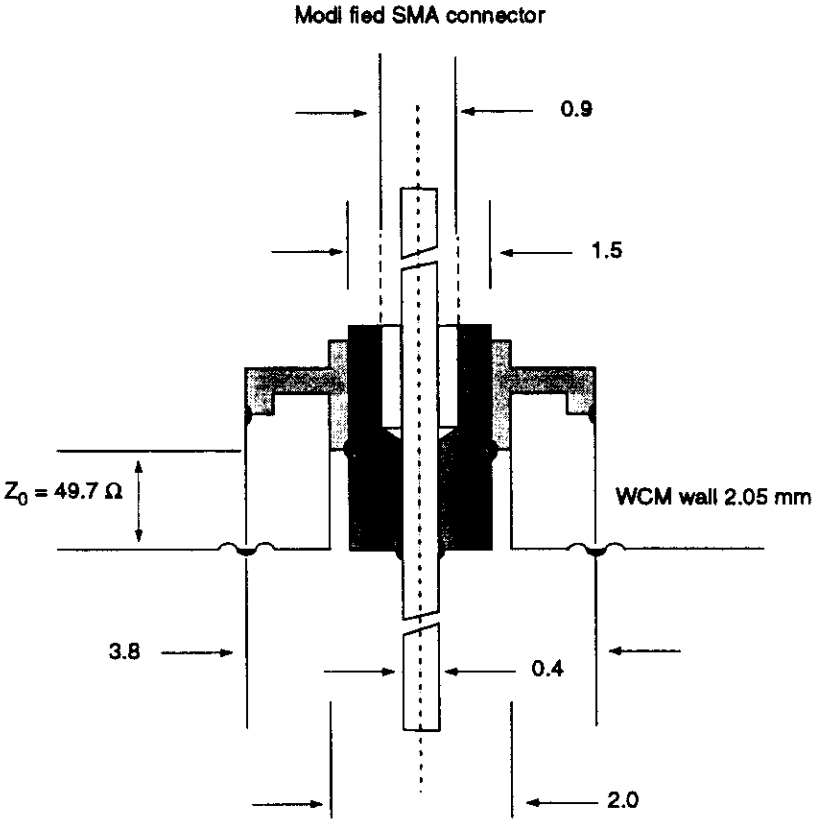

Fig. 20 The CICE feedthrough inserted inside the wall of the wall-current monitor

The TDR measurement done on the assembly described above gives a transmission rise time of 38 ps associated with a reflection coefficient VSWR = –4.8%. Further experimentation on several feedthrough assemblies confirms the importance of centring the feedthrough inside the 2 mm internal diameter coaxial adaptor to avoid a decrease of impedance value below the 50 Ω reference.

A proposal has been made to modify the CICE feedthrough to obtain further improvement with respect to UHV conditions, microwave requirements and mechanical interfacing using 2.9 mm Radiall™ 46 GHz mode-free connectors (Fig. 21).

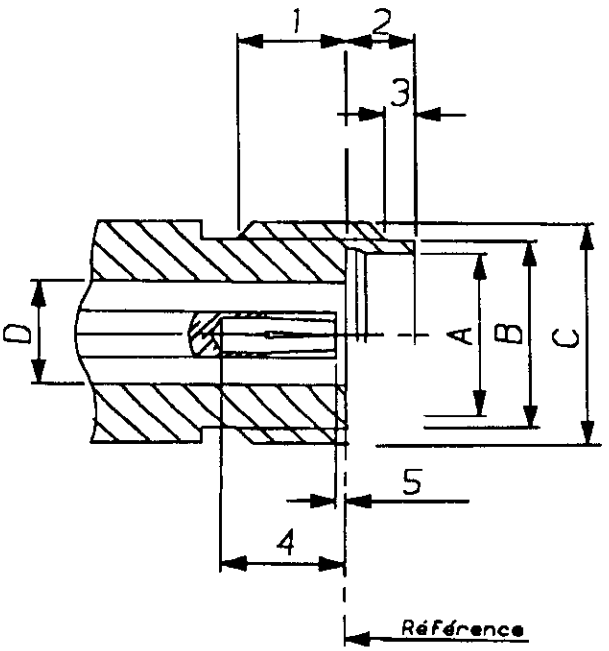

	MIN.	MAX.
1	2.87	3.27
2	1.88	1.98
3	0.38	1.15
4	2.40	3.20
A	4.60	4.63
B	5.30	5.35

Fig. 21 Modified Radiall™ 2.9 connector (machined up to the reference plane). Impedance: 50 Ω. Usable bandwidth: DC to 46 GHz. Operating temperature range: –65°C to +165°C (compatible with 150°C baking operation).

6 ARCHITECTURE AND ASSEMBLY OF THE 10 GHz WALL-CURRENT MONITOR

6.1 General description

The WCM consists of eleven different parts (Figs. 22–27).

- Two UHV flanges ① and ⑨ machined in TA6V4 material. The TA6V4 ① flange supports also the ZN tiles and the microstrip/gap assembly.
- This microstrip/gap assembly ② is a piece of copper held on the flange ① by some small (1 mm diameter) copper rivets inserted inside holes ③.
- A shielding chamber ④ made of TA6V4 material. This shielding makes an insulation between inside (beam image current) and outside (parasitic currents from environment) worlds. The wall thickness of the shielding chamber is sufficient to give this insulation inside the whole bandwidth of the WCM (skin effect).
- The T40 feedthrough ring ⑤ supports the CICE height feedthroughs and the SMA connectors.
- A sliding copper ground plane ⑩ fitted with two RF contacts ⑪ insures a quasi perfect ground reference for the microstrip/gap assembly and is, in addition, a means of impedance adjustment for the transmission line.

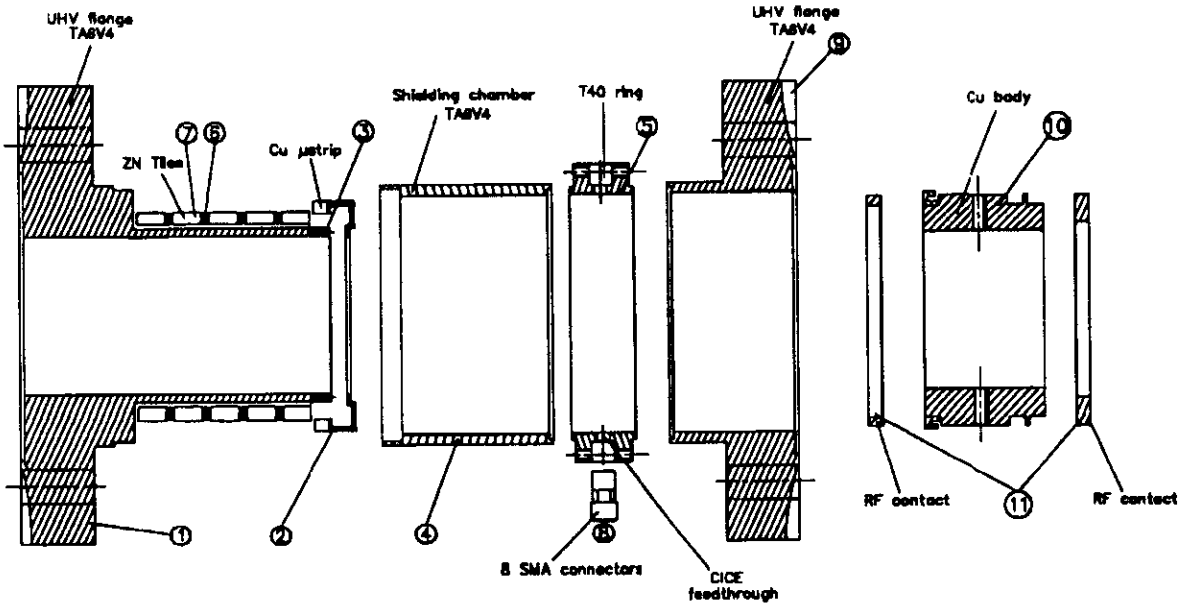

Fig. 22 The 10 GHz WCM assembly

Fig. 23 All the parts of the 10 GHz WCM

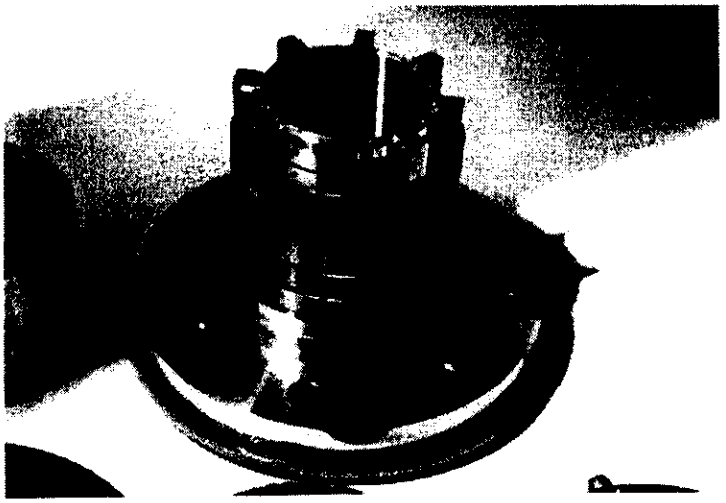

Fig. 24 Inside the WCM: the NZ2 tiles and microstrip/gap assembly

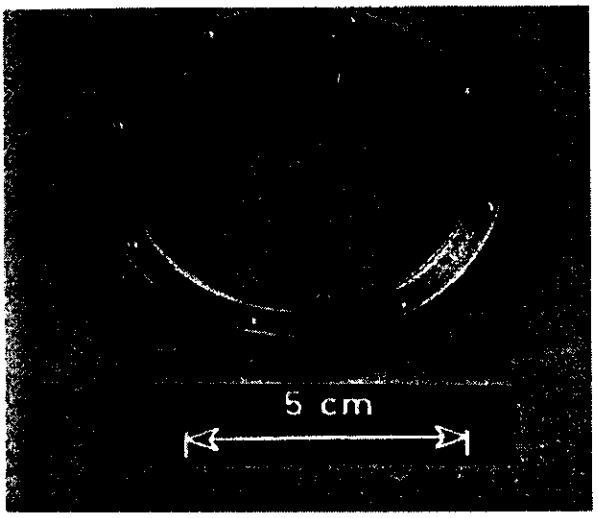

Fig. 25 The feedthrough ring and CICE devices

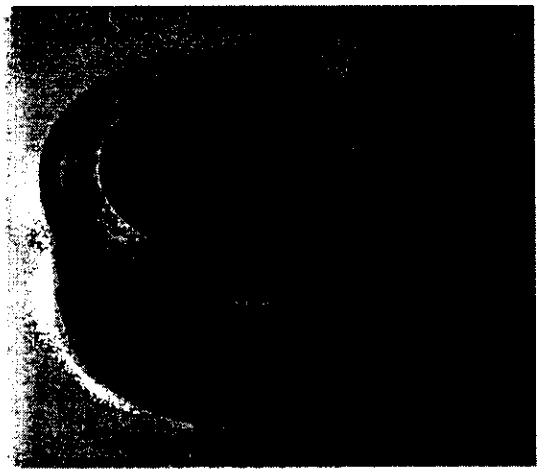

Fig. 26 The copper sliding ground plane fitted with a RF contact

Fig. 27 The 10 GHz WCM ready for operation

6.2 Assembly technology

The specificity of the wall-current monitor lies in its particular geometry designed around the CICE feedthrough.

The study done on the shape and the quality factors required shows the Electron-Beam Welding (EBW) technology to be the method the best adapted for the assembly of the various parts of the monitor.

6.3 Assembly specifications

The vacuum chamber of the WCM must be kept within a shape tolerance of ±0.05 mm. The surface finish must be UHV tight and need not be lower than the machining specifications. The intrinsic parameters of the miniature CICE feedthrough have to be preserved.

6.4 Constraints

6.4.1 Machining constraint

The titanium parts have to be machined from bulky material. The machining tolerances on the manufacturing have to be kept high for the WCM and to ensure a perfect accosting of the welded joints. The surface finish has to meet the quality standard N5 for all the functional surfaces.

6.4.2 Thermal constraint

Under welding conditions, the critical link is the welding of the miniature CICE feedthrough on the feedthrough ring ⑤. The welding energy may create a crack at the interface between alumina and titanium. Tools made of aluminium alloy are used here as thermal regulators.

The heat treatment under vacuum for the whole WCM is:

$$t = 150°C/72 \text{ hours at } p = 10^{-7} T .$$

6.4.3 Localization constraint

All the welding operations are performed inside the work piece except the last weld which closes the monitor. This is done to avoid virtual vacuum leakage as well as a microwave current circulation path (skin effect). The welding joints are inclined (Figs. 30–32).

6.4.4 Constraint of welding qualification

The WCM welding does not fall under the heading welding qualification. The welding parameters are evaluated on-line.

6.4.5 Handling constraint

During the whole assembly process the handling is done with gloves to avoid oxidization. The CICE feedthrough alumina is protected against any metallic evaporation during the welding operation.

6.4.6 The choice of materials

The CICE feedthrough is definitely the starting point of the design. It prescribes titanium as the basic material for the whole design. As briefly described above, the feedthrough ring ⑤ and the coaxial adaptor (Fig. 25) have to be made of T40 material. The T40 welding specification is adequate and its mechanical characteristics are satisfactory.

The UHV flanges are made of titanium alloy TA6V4. This choice is to guarantee good mechanical behaviour of the monitor. Its hardness, as previously noted, allows multiple compressions for replacement of UHV joints, which is of primary importance from the

experiment and maintenance points of view. The welding of titanium T40 and TA6V4 is of good quality.

Table 1 gives the composition of these materials.

Table 1

	Al	V	C	H_2	N_2	Fe	O_2	Re 0.2	A%
T40			0.08	0.015	0.05	0.12	< 0.3	29	22
TA6V4	6	4						90	8

The thermal and electrical conductivity of T40 and TA6V4 are low. The expansion coefficient is an average one. The high solubility of oxygen and hydrogen during the fusion has to be noted.

The NZ2 Emerson & Cumming tiles are known for their good behaviour under UHV conditions.

They are put under a full cleaning and baking cycle before insertion inside the WCM.

Thin copper spacers are inserted between the NZ2 slides to improve pumping performance.

6.4.7 Surface treatment

The whole cleaning cycle for the titanium parts is:

– Immersion in a non-alkaline detergent solution with a five-minute ultrasonic agitation.
– Rinsing with demineralized water.
– Immersion in demineralized water with ultrasonic agitation (5 min).
– Baking operation up to 90°C.
– Packaging before welding under argon atmosphere.

6.4.8 Assembling the wall-current monitor

The following operations are required for the assembly of the WCM:

op1: Electron-beam welding of the coaxial adaptors on the CICE feedthroughs.
op2: Electron-beam welding of the CICE feedthroughs on the feedthrough ring ⑤.
op3: UHV tests for the above parts.
op4: Electron-beam welding of the feedthrough ring ⑤ on one side with the UHV flange (and on the other side with the shielding chamber ④).
op5: UHV tests for the above parts.
op6: Assembly of the ZN2 tiles, copper spacers and microstrip lines/gap ② on the WCM body ①.
op7: Electron-beam welding of the UHV flange 1. This is the only weld outside the monitor.
op8: UHV test for the whole WCM before electrical measurements.

6.4.9 Electron-beam welding operation

a) The EBW machine used is a high-voltage PRT™ 1200/7.5 with the following gun characteristics:

Heating surface	1.4 mm^2
I_{max}	50 mA
High voltage max.	150 kV
Beam max. power	7.5 kW
Gun welding pressure	5×10^{-6} mbar
Pressure inside enclosure	5×10^{-4} mbar

b) All the joints are butt welded (Fig. 28).

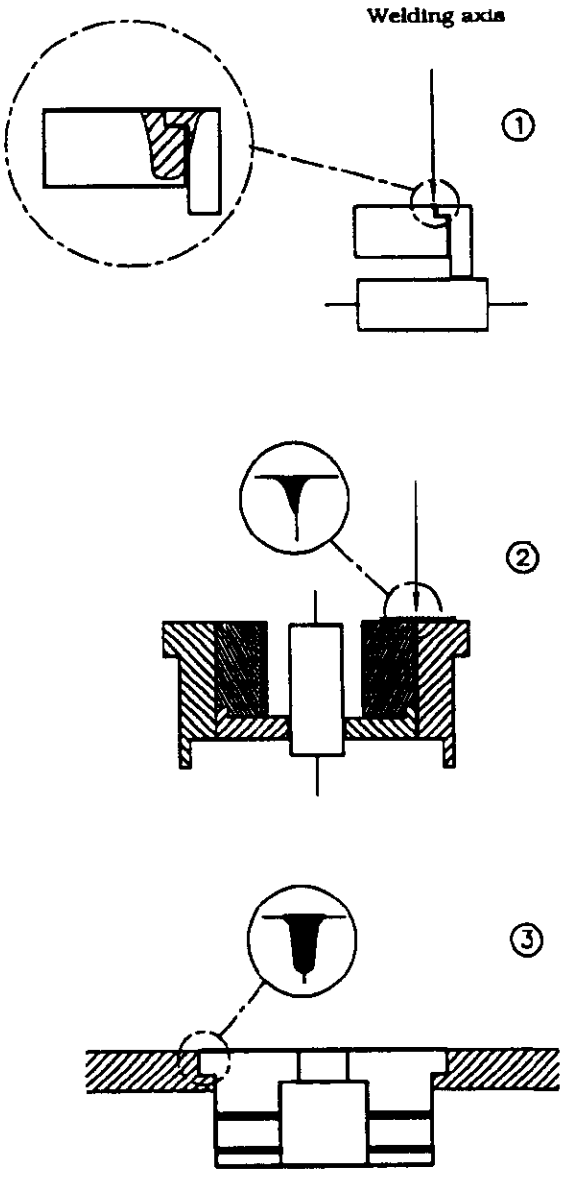

Fig. 28

c) Tool sets and rotational devices

The welding operations require specific tooling. The following refers sequentially to the assembling operations described in paragraph 6.4.8.

op1: An aluminium clamp holds the coaxial adaptor encased on the CICE feedthrough. A good contact between the adaptor and the feedthrough increases the thermal exchange during the welding. The alignment error is less than 0.05 mm. The rotational device has a tilt of 10° (Fig. 29).

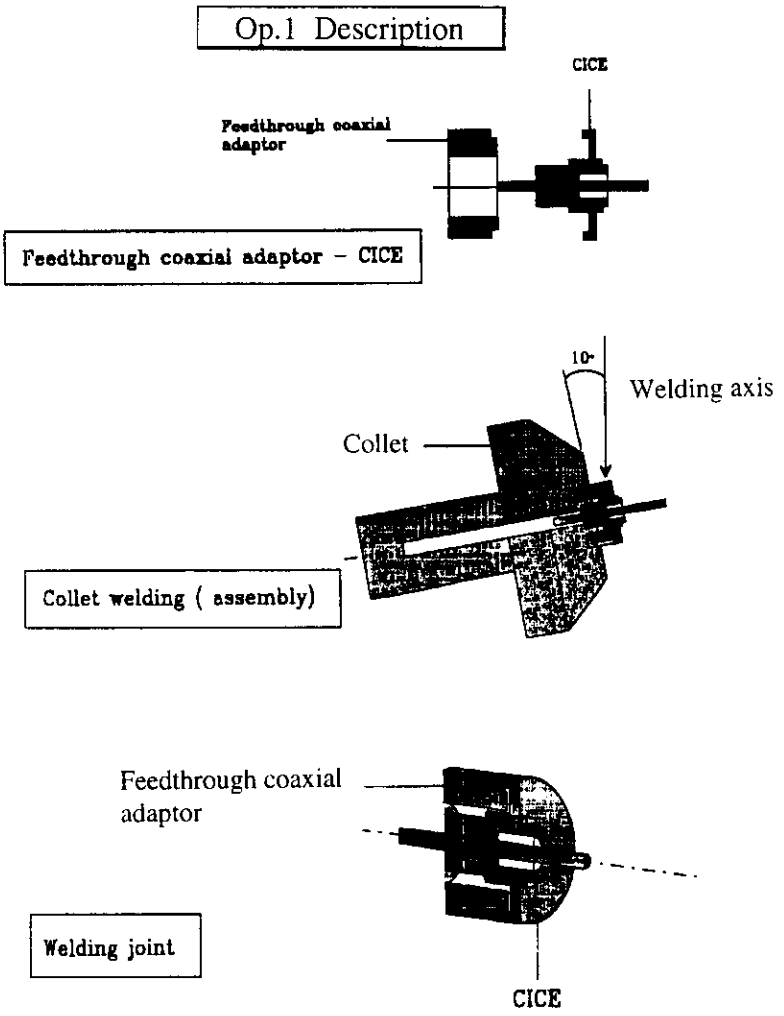

Fig. 29

op2: Tools give a perfect positioning for all the feedthroughs. The circular movement is generated by the X–Y table not the rotary axis (Fig. 30).

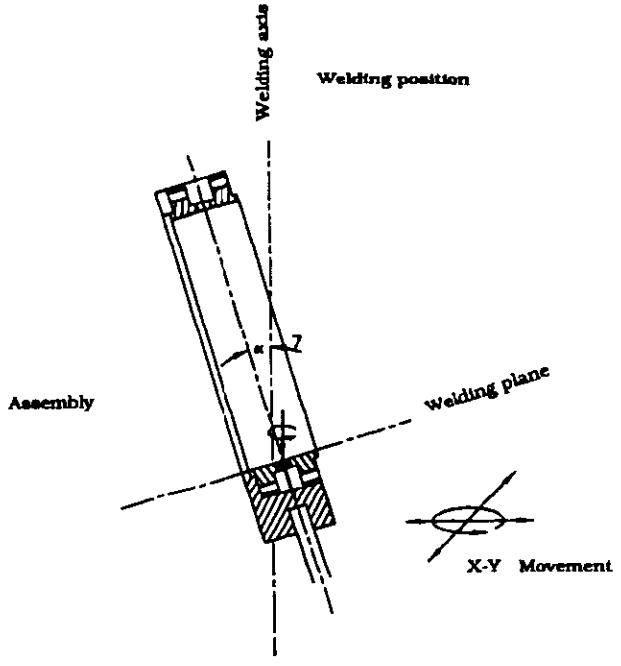

Fig. 30 Circular movement by X–Y table

op4: The parts to be welded are held by the rotational axis chuck.

d) The welding operations

All the welding operations are monitored on a real-time basis by using optical equipment. The beam in relation to joint and the adjustment of the welding parameters (Appendix 2) are corrected manually by the operator during the process.

op1: The CICE feedthrough is adjusted on the coaxial adaptor. Two welds spaced at 180° join the two parts. This is done manually. The welding cycle is manual. The circular welding is done with one pass, manually controlled. The seam is smooth and bright.

Welding parameters: It is a compromise between 'key hole' welding and thermal conduction welding.

op2: The feedthrough assembly is fitted inside the feedthrough ring ⑤ without any more machining. As described previously, two welding points hold the assembly. This is also a manual operation. The circular welding is done automatically with one pass. The seam is smooth and flat.

Welding parameters: Use of a vibrating beam of the circular kind. The bath width completely covers the joint during the displacement (Fig. 31).

Welding the CICE assembly on the feedthrough ring ⑤

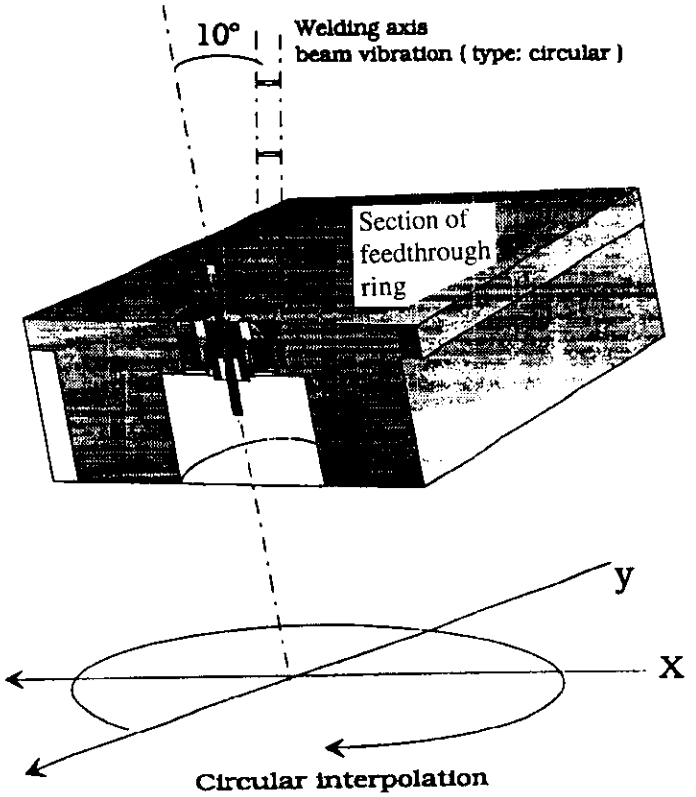

Fig. 31

op4: The feedthrough ring ⑤ is welded on the shielding chamber ④ and the UHV flange ⑨. Two welding points 10 mm long at 180° hold the position of the assembly. The seams are flat without any deformation.

Welding parameters: Use of a vibrating non-focused beam to obtain a good penetration and a smooth weld seam. The welding program is automatic (Fig. 32).

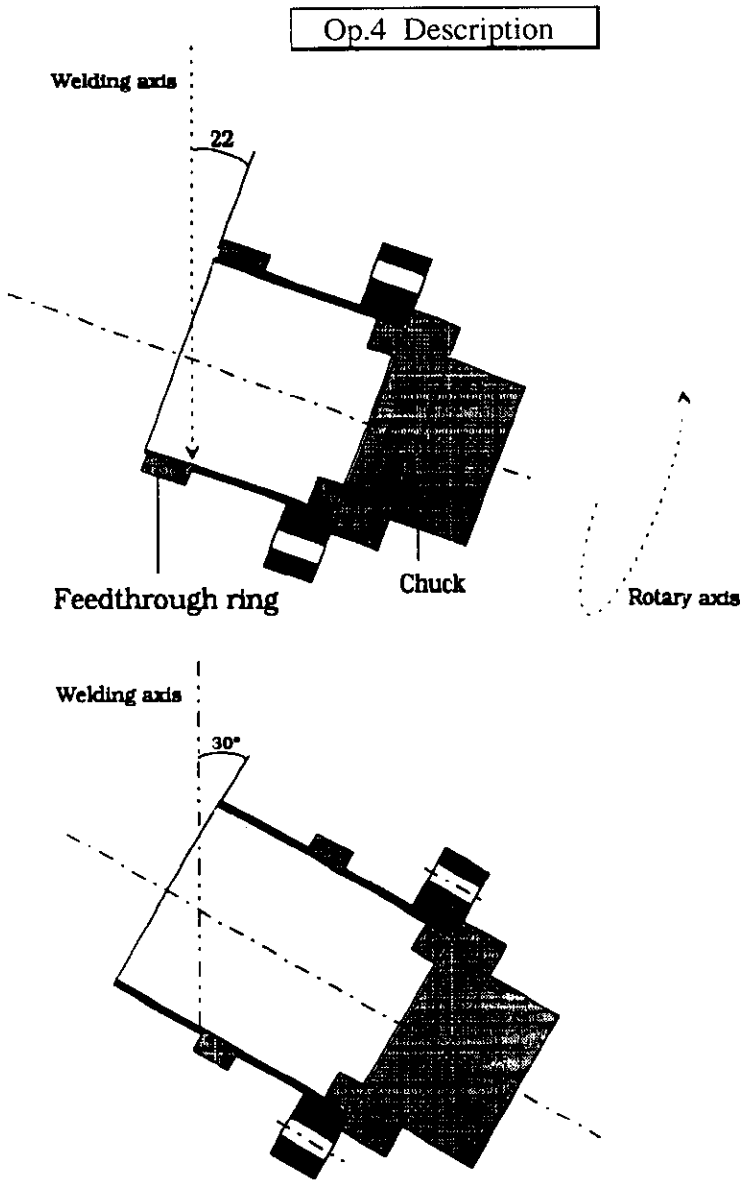

Fig. 32

op5: The WCM is finally sealed by welding on the UHV flange ①. The parameters and remarks are the same as above (op4).

6.4.10 Check

a) Visual check during welding

The weld analysis in real time allows the first observation.

The movement of the welding pool, the width of the molten zone, welding projections, also any excessive temperature rises allow the weld to be quality controlled.

The quality of the weld can only be compared with the WCM prototype.

b) Metallographic survey (Figs. 33, 34).

The only destructive testing possible is made on the weld between the CICE feedthrough and the feedthrough coaxial adaptor. The micrographic examination of the weld zone shows a very good compactness, with an homogeneous microstructure. The weld has 100% penetration without any deformation of the assembly. The heat-affected zone (HAZ) is hardly visible. The physical–chemical continuity is perfect and corresponds to the physical requirements of the assembly.

The WCM is finally checked for UHV leakage before installation on the measurement line.

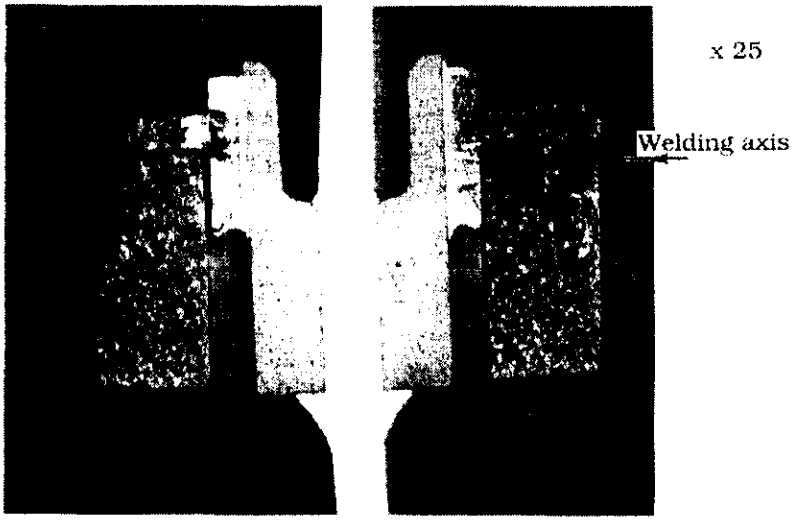

Fig. 33

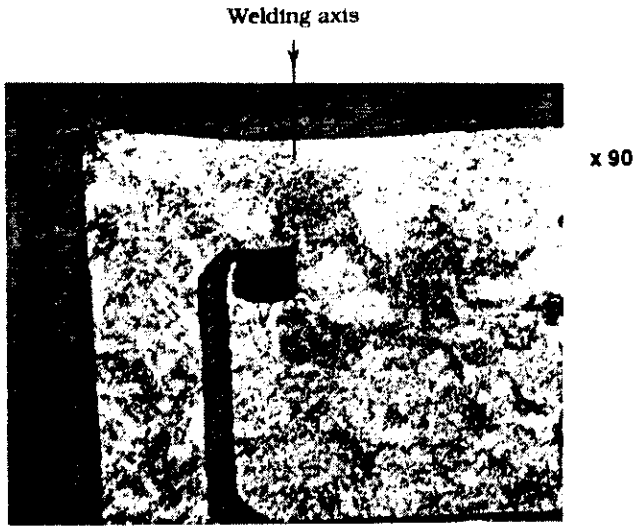

Fig. 34

7 THE 10 GHz WALL-CURRENT MONITOR ON THE TEST BENCH

1) Frequency-domain measurements are difficult to manage because moding quickly appears above 1.7 GHz with an internal diameter of 40 mm for the vacuum chamber [13].

2) Time-domain measurements using hardware time-gating (Fig. 15) prove to be a useful tool as results are quite similar to those obtained under real conditions with the e^- beam (Fig. 35).

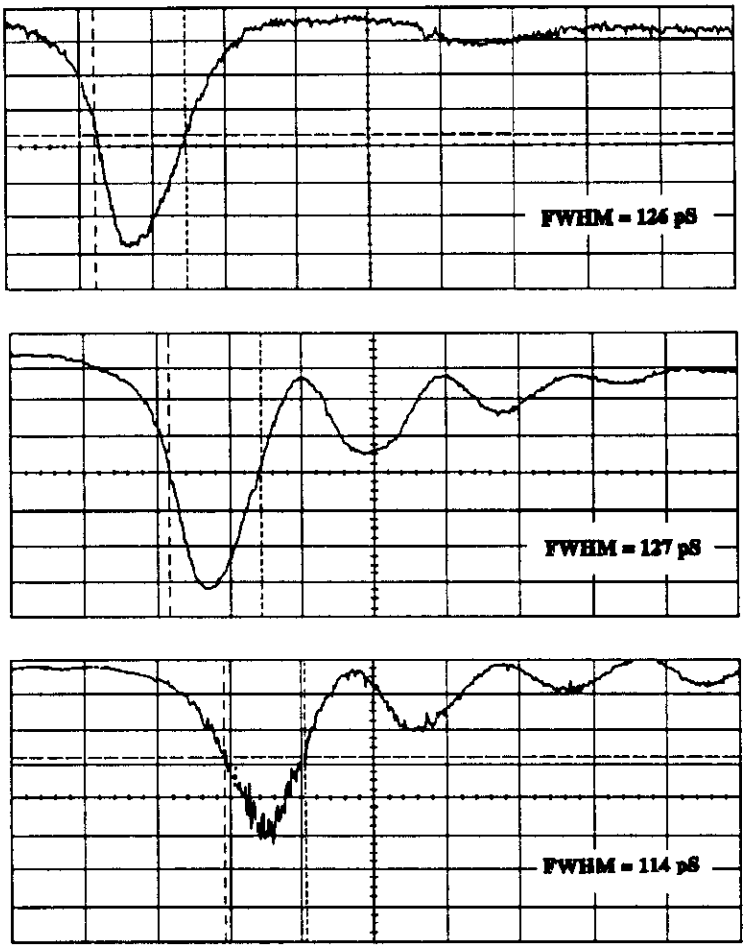

Fig. 35 Upper trace: output of the comb generator built in the HP8593A spectrum analyser. Oscilloscope HP54124T input 34 GHz. Time base: 100 ps/div. FWHM = 126 ps.
Middle trace: output of the 10 GHz WCM on the hardware time-gating test bench using the above impulse generator. Time base: 100 ps/div. FWHM = 127 ps.
Lower trace: output of the 10 GHz WCM with real e^- beam conditions. Q = 24 pC. E_c = 95 keV. Laser spot diameter = 14 mm. e^- beam standard optic. FWHM = 114 ps.
Note the same ringing as on the test bench due to imperfect matching at the CICE feedthrough.

Another alternative to the impulse condition is to inject the TDR step generator signal on the 0.5 mm diameter wire by a SMA connector located at the centre of a conical machined DN63 UHV flange. The line is assumed to be in the fundamental TEM mode (v = c) because no significant ringing is observed on the HP54124T oscilloscope display within the measurement bandwidth.

$$T_{r_{TDR}} = 36 \text{ ps} \Rightarrow \text{flight distance} = 11 \text{ mm}.$$

The measurement system response is mainly limited by the TDR step generator (Fig. 36) but includes two short 4 ns APC 3.5 Hewlett Packard cables and the rise time of the 34 GHz input of the sampler.

This 36.6 ps 10–90% rise time value will be used later to extract the wall-current monitor performance from the measurement data:

TDR rise time (step generator, cables, 34 GHz sampler input) = 36.6 ps
34 GHz sampler input alone = 10.2 ps
Wall-current monitor (as described later) $30 \text{ ps} < T_{r_{WCM}} < 45 \text{ ps}$

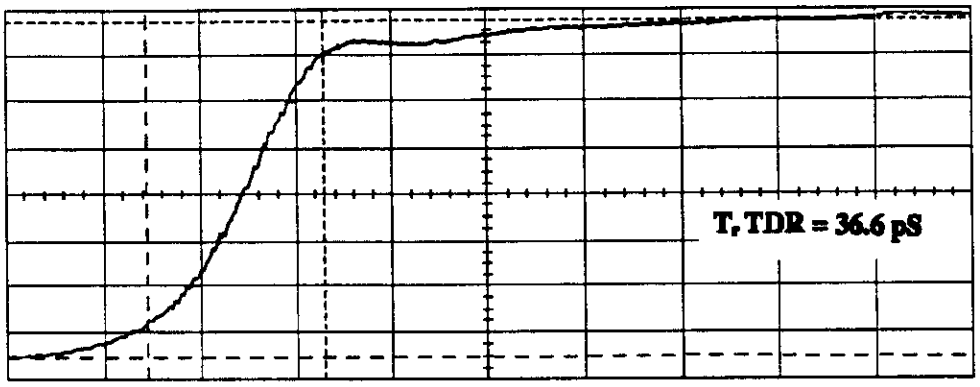

Fig. 36 TDR rise time is 36.6 ps (10–90%)

The low-frequency cut-off is measured using a 50 Ω TEM test set (Fig. 37) [12] bandwidth-limited by moding above 1.7 GHz.

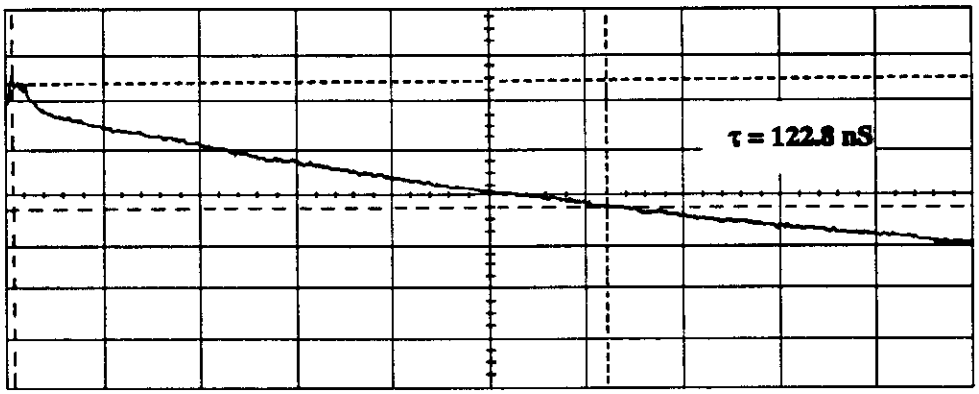

Fig. 37 Low frequency cut-off of the WCM

3) Positioning the microstrip line ground plane

The modular construction of the 10 GHz wall-current monitor allows for some positioning adjustment of the microstrip ground plane (Fig. 26). Because the mechanical completion of the copper microstrip assembly is not an easy task, microstrip bends are sharp and certainly involve more fringing capacitance than on the home-made prototype. Some deviation from the gap width nominal value (d = 2 mm) implies an increase of the standing wave ratio on the transmission lines between the gap and the CICE feedthrough (1 mm < d < 2 mm) (Fig. 38).

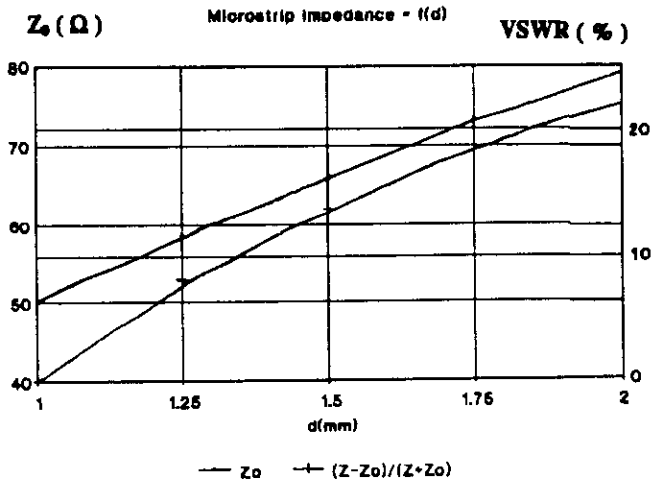

Fig. 38 Voltage standing-wave ratio and characteristic impedance of microstrip lines versus distance (d) to the ground plane

Microstrip lines are quasi TEM transmission lines. Fortunately, the dielectric constant is the same on both sides of the microstrips used and equal to unity (vacuum condition).

Moding (TE10) may appear between the microstrip and the ground plane [15].

$$F_c = \frac{c}{4d\sqrt{(E_r - 1)}} \text{ with } E_r = 1$$

d = 2 mm F_c = 37.5 GHz

d = 1 mm F_c = 75 GHz

This does not take into account the transverse mode on the microstrips. In fact, this effect seems not to interfere strongly with the behaviour of the monitor.

4) The wall-current monitor with a 2 mm gap

The parameters are the following:

Distance at the gap = 2 mm

Microstrip height versus ground = 1 mm

Theoretical microstrip impedance = 50.1 Ω

Theoretical reflection coefficient on the transmission line = 0.001%

$T_{r_{WCM}}$ = 41.7 ps ⇒ F_c = 8.4 GHz (Figs. 39–41).

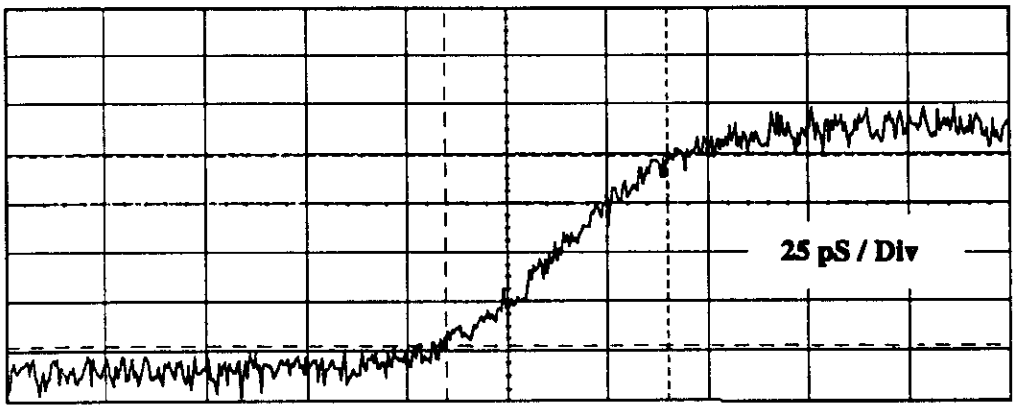

Fig. 39 Measured rise time = 55.5 ps. TDR rise time = 36.6 ps. WCM rise time = 41.7 ps. $F_{c_{WCM}}$ = 8.4 GHz. Time base = 25 ps/div.

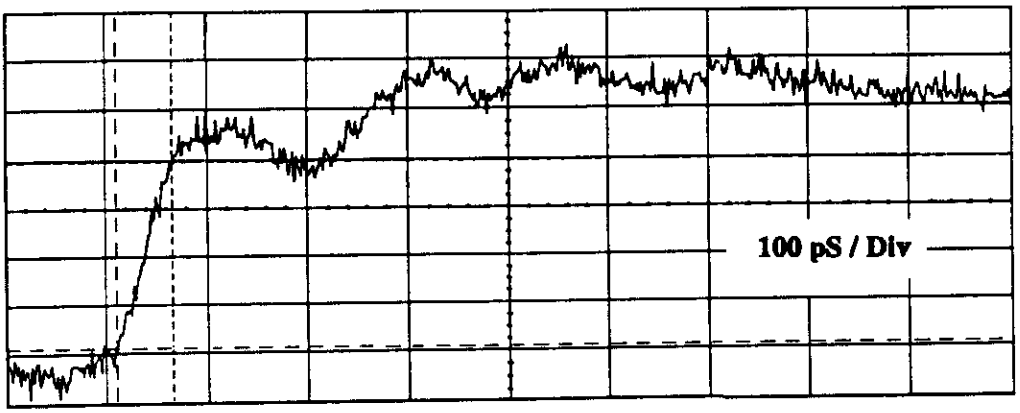

Fig. 40 Same as Fig. 39 but time base = 100 ps/div. Note the ripple on the flat top of the step because of the imperfections of the design.

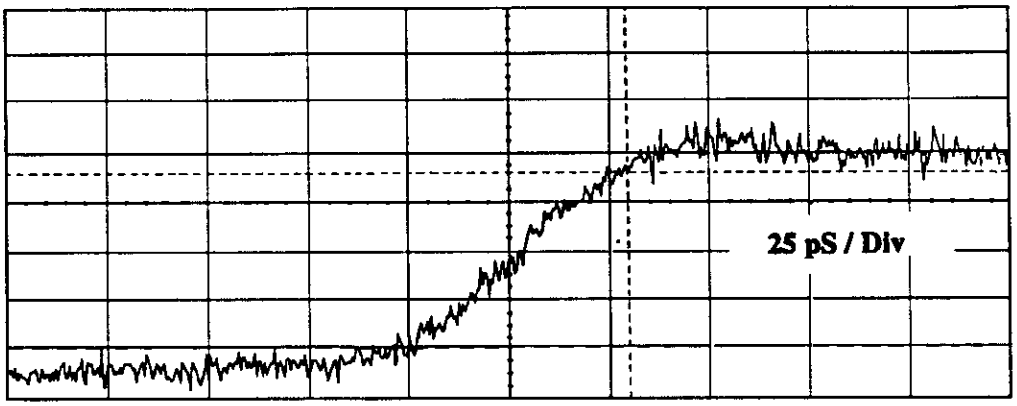

Fig. 41 Same as Fig. 39 but only one WCM output (the others loaded each by 50 Ω terminations). The combiner does not decrease the WCM performance within a 8.4 GHz bandwidth.

5) The wall-current monitor with a 3 mm gap

The parameters are the following:

Distance at the gap = 3 mm

Microstrip height versus ground = 2 mm

Theoretical microstrip impedance = 79 Ω

Theoretical reflection coefficient = 22%

$T_{r_{WCM}}$ = 32.5 ps ⇒ F_c = 10.7 GHz (Fig. 42).

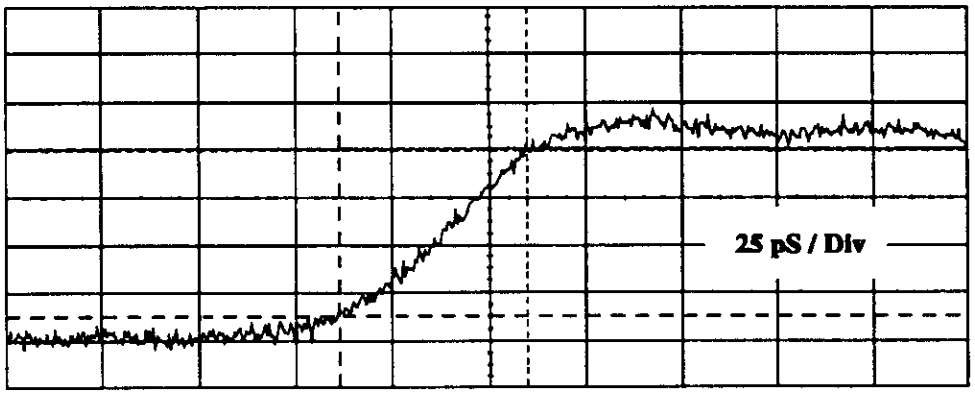

Fig. 42 Measured rise time = 49 ps. TDR rise time = 36.6 ps. WCM rise time = 32.5 ps. $F_{c_{WCM}}$ = 10.7 GHz. Time base = 25 ps/div.

The $|Z|$ transfer of the wall current monitor is measured on the 50 Ω TEM test bench (useful up to 1.7 GHz) [12] (Fig. 43).

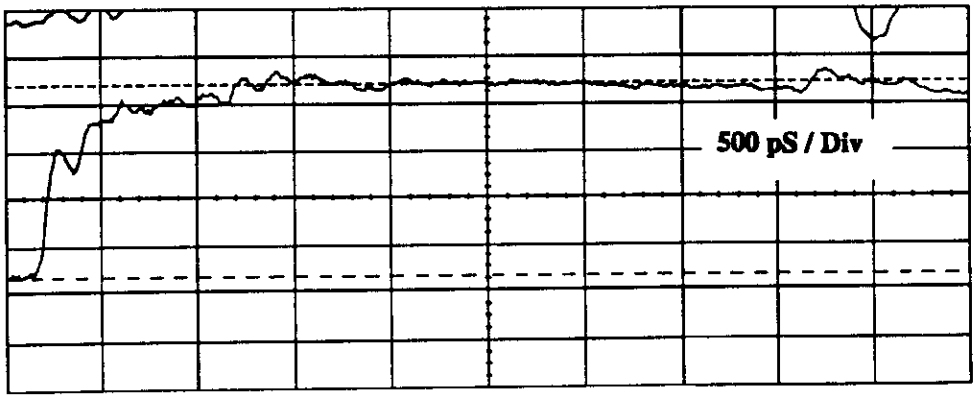

Fig. 43 At t_0 + 2.5 ns (centre of the screen): U line = 196 mV. U_{WCM} = 20.6 mV. $|Z|_{WCM}$ (well inside the bandwidth) = (U_{WCM}/U_{line}). 50 Ω = 5.25 Ω.

Note that the measurement is done well inside the bandwidth of the WCM and test bench and does not apply to the upper frequency cut-off of the monitor.

8 EXPERIMENTS AT THE PS/LP PHOTOEMISSION LABORATORY

These experiments were done in the nanosecond and picosecond range using SPECTRON™ and BMI™ lasers mentioned previously [16].

8.1 Experiments in the nanosecond range with the Nd:YAG SPECTRON™ laser

This SPECTRON™ laser is usually used to monitor the photocathode evaporation processing and to qualify the photocathodes for the CTF in the DC gun of the photoemission laboratory [17].

The measurement line is fitted with some instrumentation able to measure the e^- bunch-charge emitted from the cathode.

At the beginning of the line is a wall-current monitor with a 1.6 GHz bandwidth. This monitor is sensitive, inside its bandwidth response, to the beam image peak current. A processing module converts the WCM output signal to a DC voltage proportional to the e^- bunch-charge. This module is used with the corresponding calibration factor for the experiments with the 10 GHz WCM.

At the end of the measurement line is a Faraday cup whose output voltage $U_{fc} = Q/C_{fc}$ is directly proportional to the e^- bunch-charge.

Multiple real-time data-acquisition is done by computer [18].

Figure 44 shows the WCM output under the following nanosecond conditions:

Gun_{HT} = 95 kV

I_{coils} 1, 2, 3, 4 = 2.7 A, 2 A, 1.8 A, 1 A

Q measured at the WCM = 32.1 nC

Q measured at the Faraday cup = 28.5 nC

Charge transmission across the measurement line = 88.8%.

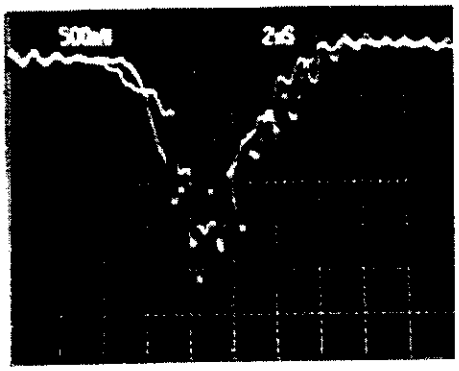

Fig. 44 The WCM output under nanosecond conditions. Attenuation = 26 dB. U peak = 44.5 V. FWHM = 4 ns. Oscilloscope 7104/BW = 1 GHz.

8.2 Experiments in the picosecond range with the BMI™ laser

The conditions for experiments are the following.

Instrumentation: Sampling oscilloscope HP54124T input 34 GHz;
Low-loss 4 ns HP cable;
HP 26.5 GHz 20 dB attenuators;
Trigger from a 150 ps vacuum photodiode 16 ns at least before signal.

Optical delay on the 262 nm laser path.

There are several contributions to the stretching of the e^- bunch in such a DC gun:

The divergence of the gun seen at 240 mm by the WCM;

The space-charge effects;

The time dispersion introduced by the e^- beam optic (coil number 1);

The FWHM laser pulse and the relaxation time of the photocathode are known parameters.

Figures 45–47 show the results of these cumulative effects, including the bandwidth limitation introduced by the WCM and the sampling scope instrumentation, for a laser spot of 14 mm diameter. The laser spot is visually assumed to be without 'hot spots'.

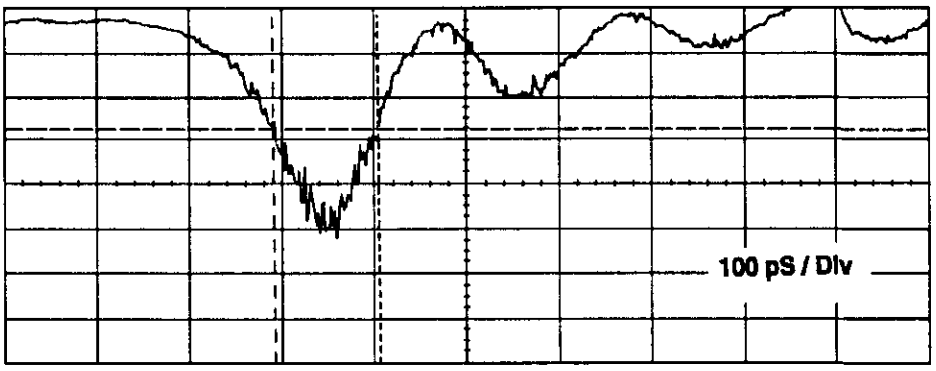

Fig. 45 The WCM output under picosecond conditions. Laser spot = 14 mm diameter. E_c = 95 keV. Standard optic. Q_{FC} = 24 pC. FWHM = 114 ps. Time base = 100 ps/div.

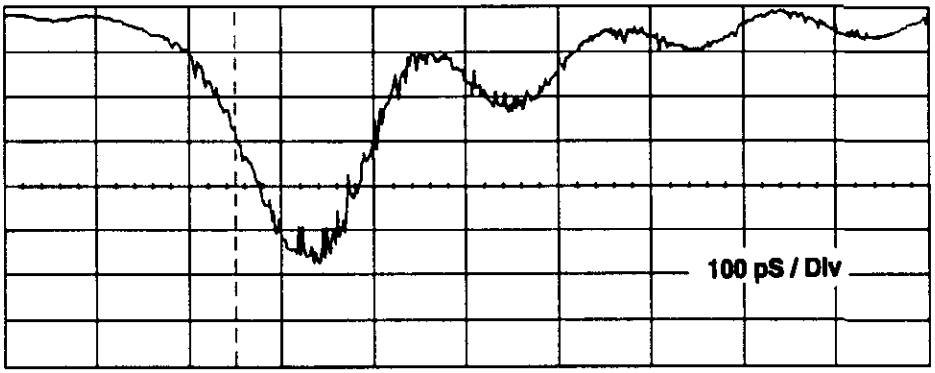

Fig. 46 WCM output with the same condition as Fig. 45 but Q_{FC} = 280 ps. FWHM = 150 ps. Time base = 100 ps/div.

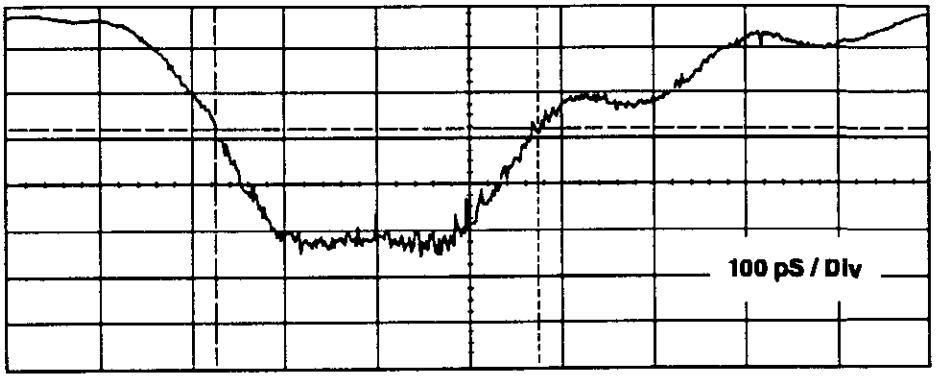

Fig. 47 WCM output with the same conditions as Fig. 45 but Q_{FC} = 3 nC. FWHM = 350 ps. Time base = 100 ps/div.

An attempt to dissociate the effects was done by keeping the laser diameter and the bunch charge constant, putting all the coil currents to zero and doing a scan of the gun high voltage (Fig. 48).

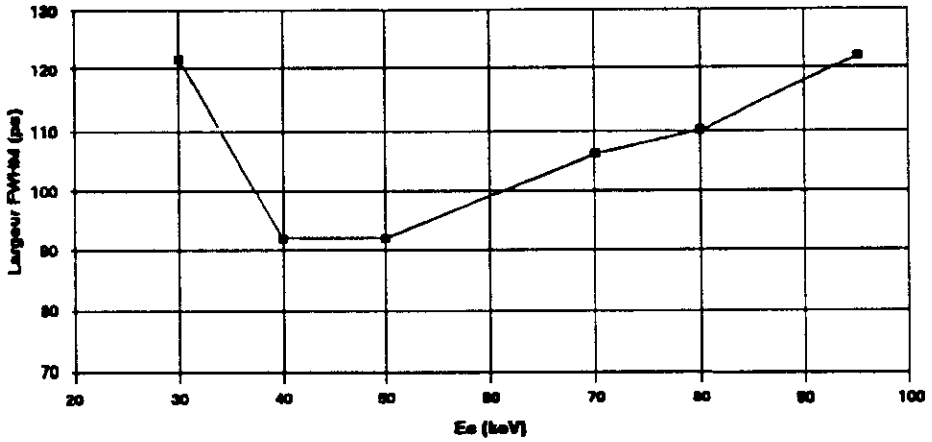

Fig. 48 FWHM e^- bunch = f (E_c). Q_{e^-} = C' = 14 pC. Laser spot diameter = 14 mm. I_{coils} = 0.

The bunch charge is kept low (about 14 pC) to limit as far as possibe the space-charge effect.

Figure 49 shows the typical WCM output with E_c = 50 keV.

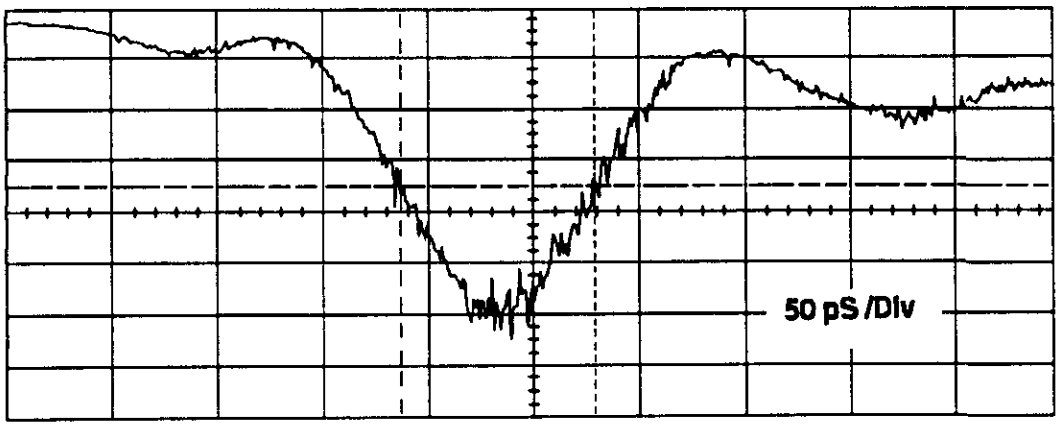

Fig. 49 WCM output. E_c = 50 keV. Q_{e^-} = 14 pC. Laser spot = 14 mm. I_{coils} = 0. FWHM = 92 ps.

Figure 50 shows the typical WCM output with E_c = 45 keV and a low charge value.

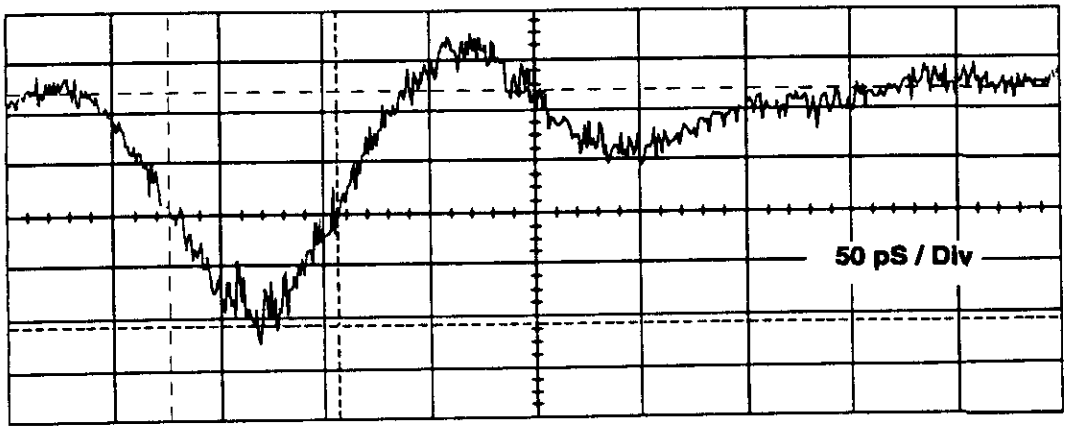

Fig. 50 Same as Fig. 49 but E_c = 45 keV. FWHM = 80 ps.

The 10 GHz wall-current monitor fulfils all the requirements (sensitivity, bandwidth, overshoot) for single and multiple-bunch (Δt_{min} = 330 ps) operation experiments at the Photoemission Laboratory.

9 AN ATTEMPT AT ADAPTATION OF THE WALL-CURRENT MONITOR TO THE CLIC TEST FACILITY

An attempt at adaptation of the WCM is possible with this kind of modular construction (sliding copper ground plane).

This copper ground plane ⑩ (Fig. 51) is modified to fit a molybdenum wire ring at one of its ends.

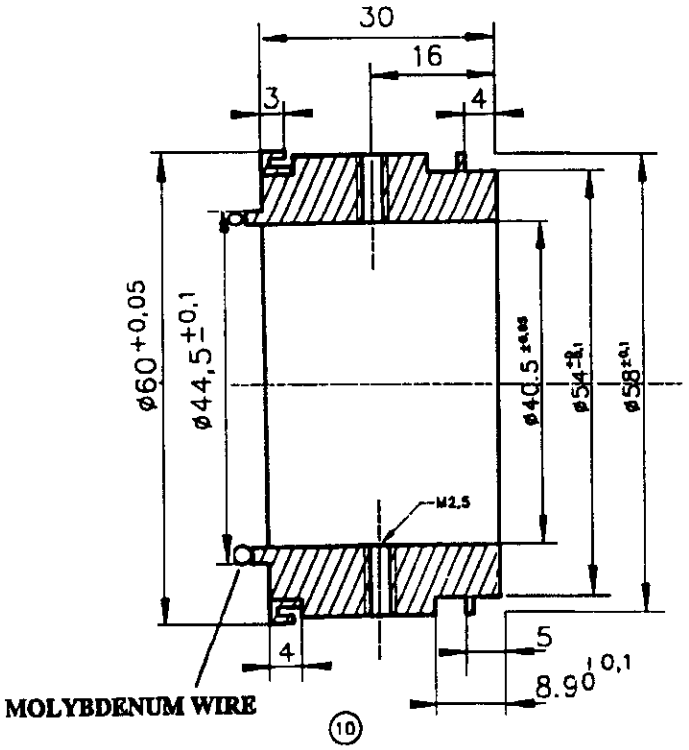

Fig. 51 Modifying the copper ground plane

This molybdenum wire ring is a low-impedance short circuit at the gap, estimated to be in the range 10–100 mΩ.

The WCM is installed in the Clic Test Facility, at atmospheric pressure, just behind the vacuum chamber membrane. A luminescent screen allows for the e^- beam position visual check just after the WCM.

The HP54124T 34 GHz scope input is used with a HP54008A 20 GHz 22 ns delay line. With this scheme, the instrumentation is triggered by the incoming signal from the WCM.

The connection from the CTF accelerator to the outside world is done by an eight-metre-long CK50 HUBER & SUHNER low-loss coaxial cable (Appendix 3).

The most significant test is done with the following parameter values:

One-bunch operation

Q bunch = 1.8 nC FWHM = 8 ps

I_{beam} = 225 A

U_{WCM} = 6 V peak

$|Z_t|_{WCM} = U_{WCM}/I_{beam}$ = 25 mΩ at the observation place.

It appears an unsuitable situation for bunch-to-bunch charge measurement (Figs. 52, 53).

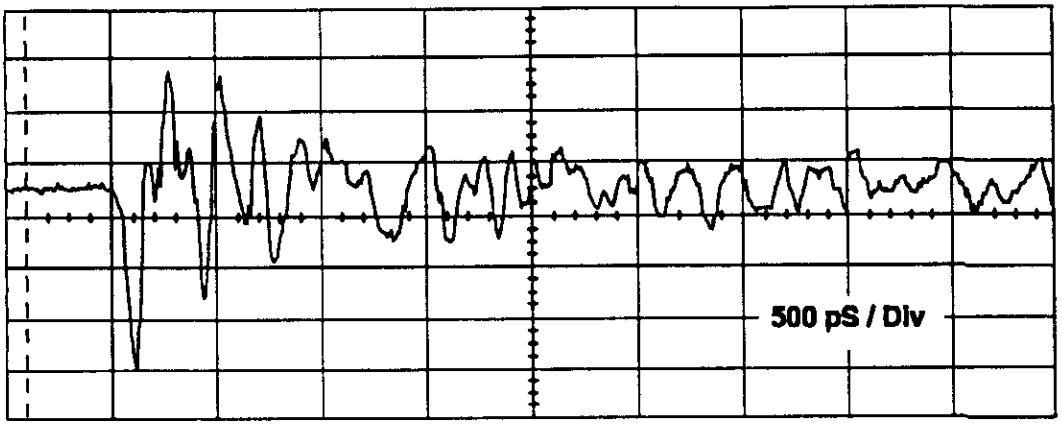

Fig. 52 WCM output under CTF conditions. Time base = 500 ps/div. 2 V/div. One-bunch (Q = 1.8 nC).

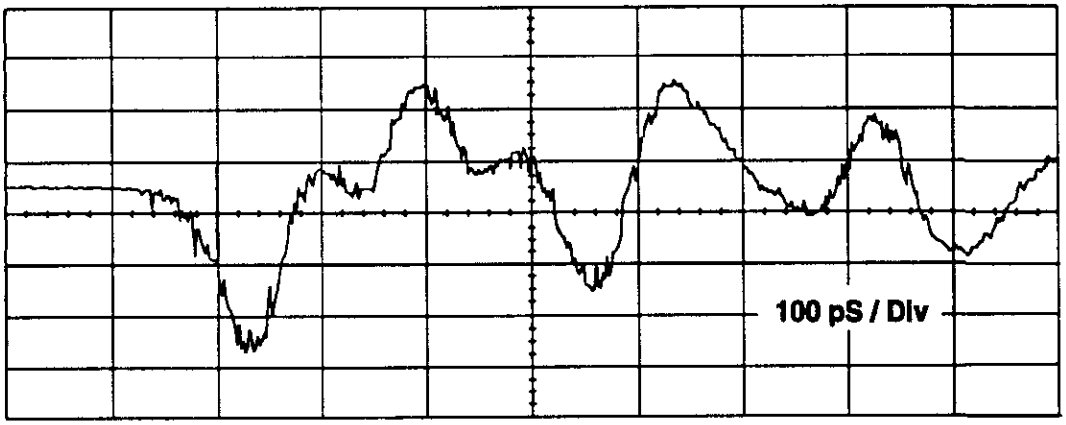

Fig. 53 Same as Fig. 52 but: Time base = 100 ps/siv. 2 V/div. One-bunch (Q = 1.8 nC).

An attempt to improve grounding of the WCM to the vacuum chamber proved to be unsuccessful. To obtain a better understanding of the behaviour of a 'short-circuited' WCM, the monitor is fitted on the wire test bench previously described (Fig. 15).

The situation obtained under CTF beam conditions is reproduced on the test bench using the HP8593 spectrum analyser built-in comb generator (Fig. 54) (Appendix 3).

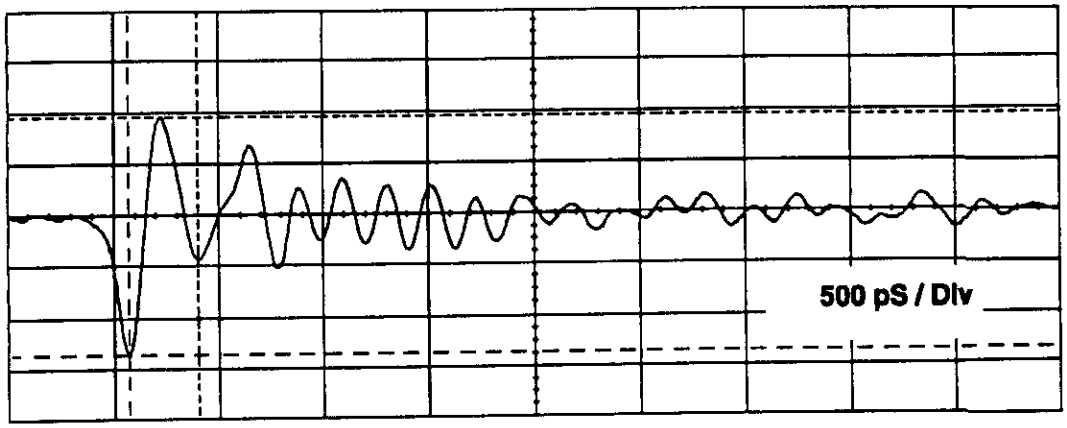

Fig. 54 Output of the short-circuited WCM on the test bench. Time base = 500 ps/div. Δt = 330 ps. WCM output number 5.

In fact, the analysis of each of the eight outputs shows dispersive waveforms. Further investigation with the TDR gives a strong indication that such a low impedance is difficult to obtain at the gap and leave place for improvement (Fig. 55).

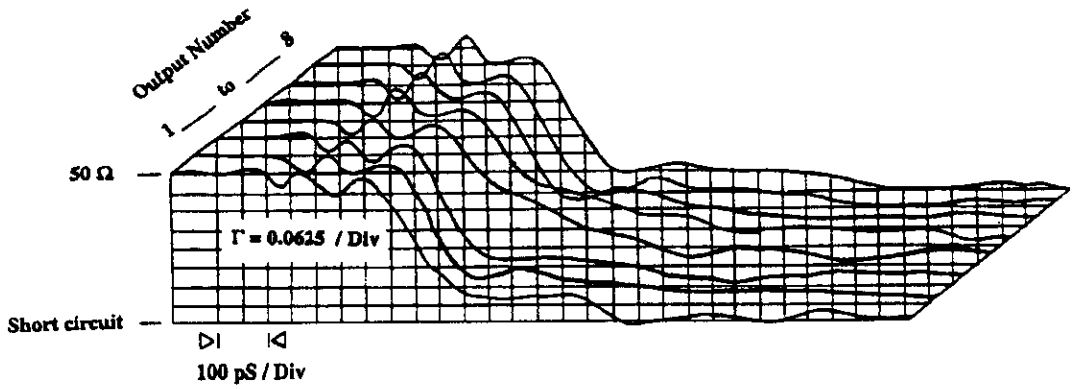

Fig. 55 TDR analysis of the eight outputs of the shortcircuited WCM

Such an effect is easily seen on outputs 4 and 5. Some mechanical improvements have to be made to obtain similar pattern characteristics all around the gap. It is also obvious that the molybdenum short-circuit at the gap appears as a quasi ideal voltage source for the microstrip transmission line and the CICE feedthrough. This necessitates a better microwave matching on the microstrip transmission line and CICE feedthrough.

10 CONCLUSION

From these designs and experiments it becomes more evident that a miniature UHV feedthrough is the key for wideband monitor applications.

This 10 GHz wall-current monitor covers a four-decade bandwidth and a five-decade charge dynamic range. It also fulfils the measurement requirements for single-bunch and multiple-bunch picosecond and nanosecond applications at the PS/LP Photoemission Laboratory.

The straight translation of the design to the Clic Test Facility applications did not work straightaway, but some experience has been gained on the subject of kiloamp–picosecond beam instrumentation.

Multiple-bunch operation will require more improvement of the design towards a ringing-free monitor usable for CTF.

ACKNOWLEDGEMENTS

The authors are particularly grateful to M. Gaillard and R. Trabelsi of CICE for fruitful discussions and the AM9210 samples for the experiment.

APPENDIX 1

INDUCTANCE OF STRAIGHT WIRE

A usual equation is:

$$L(\mu H)=0.0021\left[2.3\log_{10}\left(\frac{4l}{d}-0.75\right)\right]$$

with

l = length of the wire (cm)
d = diameter of the wire (cm).

A more precise equation [19] including skin effect is:

$$L(\mu H)=0.0021\left[\mathrm{Ln}\left(\frac{4l}{d}\right)-1+\frac{d}{2l}+\frac{\mu r\, T(x)}{4}\right]$$

with

r = d/2 (cm)
l = length of the wire (cm)
F = frequency (Hz).

T is an AC correction from tables [20].
T is approximated by curve fitting with a precision of a few per cent for $0 \le x \le 100$.

$$T(x)=\sqrt{\frac{0.873011+0.00186128x}{1+(-0.278381x)+0.127964x^2}}$$

with

$$x=2\pi\sqrt{\left(\frac{2\mu F}{\sigma}\right)}\ ,$$

σ = *conductivity*.

APPENDIX 2

ELECTRON-BEAM WELDING PARAMETERS

CERN Division MT Group MF Job: **ELECTRON-BEAM WELDING** **Leybold 7.5 kW 150 kV**	WCM			
Material	T40	T40–TA6V4	TA6V4	TA6V4
Parameters (Leybold machine)	Operat. 1	Operat. 2	Operat. 3	Operat. 4
Cathode heating current (A)	1.37	1.37	1.37	1.37
Accelerating voltage (kV)	100	100	100	100
Beam current (arb. units)	Manual	240	650	650
Focusing current on the work piece (arb. units)		3200	3200	3200
Focusing current used during welding (arb. units)	Manual	3200	3150	3150
Welding speed (mm/s)	20	10	15.5	14.5
Work piece diameter (mm)	4	4	60	60
Advance speed, axis XY (arb. units) Circumference (mm) Welding time (s) Advance speed of rotary axis (arb. units)		598.8	 188.4 12.15 1809.98	 188.4 12.99 1693.21
Working distance (mm)	150	150	150	150
Penetration (mm)	**0.4**	**0.4**	**1**	**1**
Up slope (mm)	1	1	10	10
Down slope (mm)	1	1	10	10
Up slope (s) Down slope (s) Up slope (degree) Down slope (degree)	0.05 0.05	0.1 0.1	0.65 0.65 19.11 19.11	0.69 0.69 19.11 19.11
Beam vibration				
Amplitude X		50	20	20
Amplitude Y		50	20	20
Frequency of vibration (Hz)		900	900	900
Type of vibration (geometry)		Circular	Circular	Circular
Parameters ISO	Operat. 1	Operat. 2	Operat. 3	Operat. 4
Accelerating voltage (kV) Beam current (mA) Focusing current of the work piece (mA) Focusing current used during welding (mA) Welding speed (mm/s) Beam power (W)	100 Manual Manual 20	100 1.2 320 320 10 120	100 3.25 320 315 15.5 325	100 3.25 320 315 14.5 325

APPENDIX 3

TRANSMISSION OF AN IMPULSE ALONG DELAY AND TRANSMISSION LINES

The possibility to observe short pulses with the 50 GHz HP54124T oscilloscope behind a lossy transmission line is evaluated using a length of about 5 metres of Huber & Suhner CK50 coaxial cable. This is the minimum length of transmission line for observation outside the particle accelerator. The oscilloscope is triggered by the incoming signal using a HP54008A delay line (22 ns delay, usable up to 20 GHz).

The equipment used is the following:

Oscilloscope HP54124T, input 34 GHz (Tr = 10.2 ps);

Attenuators HP 20dB 26.5 GHz;

Two-way power splitter 12.4 GHz Huber & Suhner;

Built-in HP8593 100 MHz repetition comb generator.

Figure 56 shows the signal output from the comb generator.

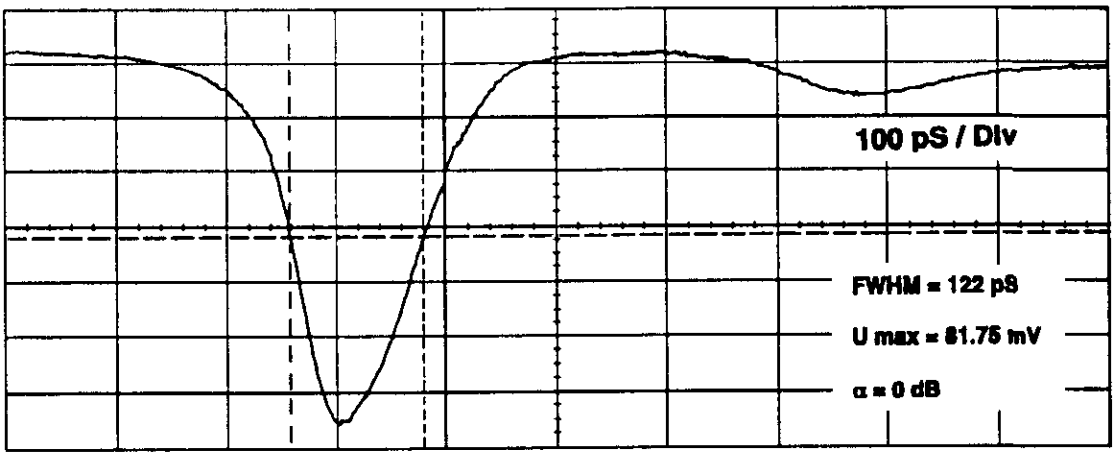

Fig. 56

Figure 57 shows the same signal after the HP54008A delay line.

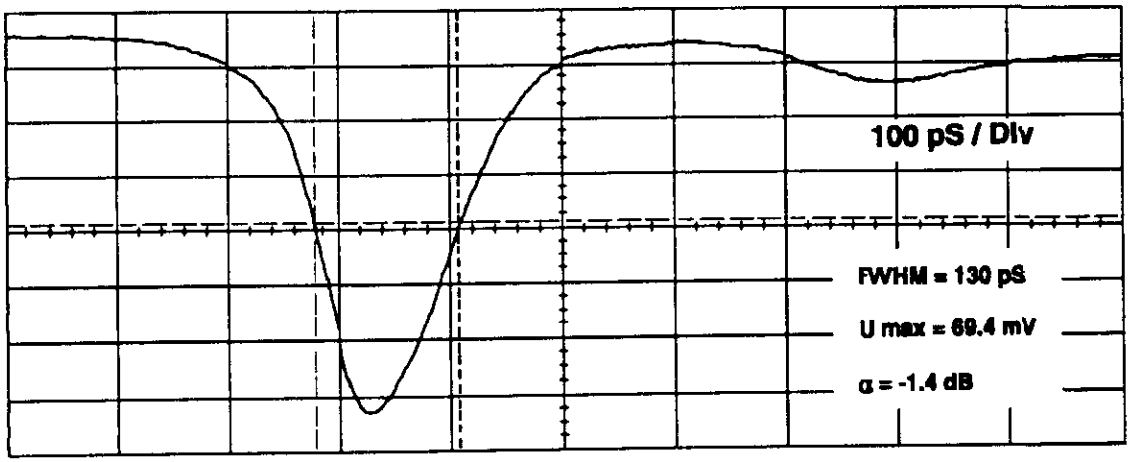

Fig. 57

Figure 58 shows the same signal after 16.7 ns of CK50 coaxial cable and the HP54008A delay line.

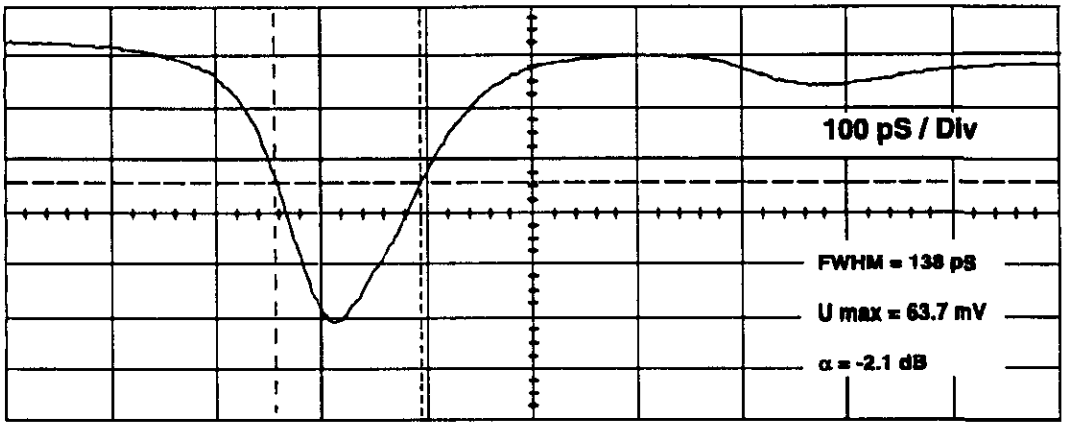

Fig. 58

REFERENCES

[1] Y. Baconnier, K. Geissler, J.H.B. Madsen, A. Pisent and G. Suberlucq, The DC test bench for laser driven photo-emissive cathode, CLIC studies, CLIC note 116, CERN/PS 90–24 (LP).

[2] Y. Baconnier, R. Bossart, K.K. Geissler, J.C. Godot, K. Hübner, H. Kugler, J.H.B. Madsen, A.J. Riche, J. Ströde and G. Suberlucq, The CERN Linear Collider Test Facility, paper presented at the 1990 Linear Accelerator Conference, Los Alamos, 1990, CERN CLIC note 119.

[3] T. Linnecar, The high frequency longitudinal and transverse pick-ups used in the SPS, CERN/SPS/ARF/78–17.

[4] J. Durand, Using a 0.5–700 MHz electrostatic pick-up at the PS/LP Photoemission Laboratory, PS/LP/note 94–25 (tech.).

[5] R. Chapput, Résolution de la mesure des micropaquets avec un wall current monitor, L.U.R.E service linac, RC/MM/ 36–90.

[6] J. Durand, Combining wideband signals from a wall current monitor, PS/LP/note 94–14 (tech.).

[7] T. Moreno, Microwave transmission design data (McGraw Hill, New York, 1948).

[8] E.O. Hammerstad, Equations for microstrip circuit design, Proceedings of the 5th European Microwave Conference, Hamburg, 1975 (Microwave Exhibitions and Publ., Sevenoaks, Kent, 1976).

[9] V. Fusco, Microwave circuits: analysis and computer-aided design (Prentice-Hall, Englewood Cliffs, N.J., 1987).

[10] International Telephone and Telegraph Corporation, New York, Reference data for radio engineers, 6th ed. (Sams, Indianapolis, 1975).

[11] TDR fundamentals for use with HP54120T digitizing oscilloscope and TDR, Hewlett Packard application note 62.

[12] J. Durand, Utilisation du wall current monitor au laboratoire de Photoemission PS/LP, PS/LP/note 91–10 (tech.).

[13] H.E. Green, Determination of the cutoff of the first higher mode in a coaxial line by a transverse resonance technique, IEEE. Trans. Microwave Theory Tech. **37**, (10) 1989, *cited in:* Transmission line design handbook, Brian C. Wadell, Artech House, Boston, 1991.

[14] P. Braham and C. Metzger, High-frequency coaxial vacuum feedthrough for the stack core stochastic cooling systems for the CERN antiproton accumulator complex, PS/AR/note 88–4.

[15] Williams, Dylan, Paananen, Suppression of resonant modes in microwave package, IEEE MTT.S symposium digest, 1989, *cited in*: Transmission line design handbook, Brian C. Wadell, Artech House, Boston, 1991.

[16] S.C. Hutchins, Photocathode lab optical system, PS/LP/Note 93–31.

[17] E. Chevallay, J. Durand, S. Hutchins, G. Suberlucq and M. Wurgel, Photocathodes tested in the dc gun of the CERN Photoemission Laboratory, Nucl. Instrum. Methods Phys. Res. **A340** (1994).

[18] E. Chevallay, Acquisit program, CERN–PS/OP.

[19] B.C. Wadell, Transmission line design handbook (Artech House, Boston, 1991).

[20] F.W. Grovers, Inductance calculations (Van Nostrand, New York, 1946).